USING NON-LINEAR FINITE ELEMENT ANALYSIS TO ANALYZE THE EFFECTS OF CONNECTION DESIGNS ON THE ICE STRENGTH OF A VESSEL

By

© Joshua Gosse, B.Eng.

A thesis submitted to the School of Graduate Studies

in partial fulfillment of the requirements for the degree of

Master of Engineering

Faculty of Engineering and Applied Science

Memorial University of Newfoundland

October 2023

St. John's Newfoundland and Labrador Canada

Abstract

As global temperatures rise, ice clears in the Arctic Ocean and the demand for Canadian Coast Guard presence in the Canadian Arctic increases. The Canadian government intends to acquire two new heavy icebreakers as part of the “Polar Icebreaker Project”. These icebreakers are to be built to IACS Polar Class 2 standards. Some classification societies require fully welded collars to support stiffener penetrations through deeper hull structure in the ice-strengthened region of the ship. This, however, is a labour-intensive, material-heavy, and thus costly way to manufacture these vessels. This study analyzes hull structural response for three alternative penetration support details and compares these with the base case for a fully welded collar. The goal is to determine if there is a more cost-effective and less material-intensive way to implement these penetrations while maintaining the stiffness of a fully welded collar. A three-dimensional model of the port side ice strengthened structure of a polar class 2 vessel was investigated. A design ice load pressure patch based on the International Association of Classification Society's unified rules for polar class was applied to the structure using finite element analysis. Results show that two of the three alternative connection designs gave unsatisfactory performance but that alternative connection designs with less steel and less welding can maintain acceptable structural strength.

Acknowledgements

I would like to thank the following people for their knowledge, guidance, and support throughout my Master of Engineering program:

1) Dr. Bruce Quinton, my graduate supervisor, for his continued support, guidance, expertise, ability to push me for more, reassurance, and positivity even during stressful times. Bruce was the perfect supervisor in every way imaginable and I am grateful that he gave me this opportunity.

2) My parents, Kim and Paul Gosse, for their unwavering love and care. They made life outside of academics far easier and provided me an outlet for anything I wanted to discuss.

3) Project partners Andrew Kendrick, Claude Daley, and James Bond for their expertise and outstanding help with my research. They laid the groundwork for the project and ensured I followed through with the best guidance possible.

4) Mark Pye, Andrew Ivany, Angie Antolinez, and brother Nick Gosse for their constant support and ability to help me take my mind off research and have fun.

5) The MUN department of Ocean and Naval Architectural Engineering for allowing me to persevere in my naval research and career.

Table of Contents

List of Tables

List of Figures

List of Symbols, Nomenclature, or Abbreviations

ABS	American Bureau of Shipping
ASCII	American Standard Code for Information Exchange
B-T	Belytschko-Tsay
CBS	Centred Between Stringers
COS	Centred on Stringer
DOF	Degrees of Freedom
DWL	Design Waterline
FEA	Finite Element Analysis
H-L	Hughes-Liu
IACS	International Association of Classification Societies
MCA	Mesh Convergence Analysis
NIP	Number of Through-Thickness Integration Points
PC	Polar Class
PWBS	Product-Oriented Work Breakdown Structure
SHRF	Shear Correction Factor
SWBS	Systems-Oriented Work Breakdown Structure
UR	Unified Rules
W1S	Penetration Welded on One Side

List of Appendices

Chapter 1 Introduction

Design approaches for connections in ice-class ships are typically based on standard practices for other structural design. Many of these standard practices stem from sets of rules developed over time from various Classification Societies. As technology has advanced and more was learned about strength of ships in ice, the International Association of Classification Societies (IACS) developed a set of unified polar requirements (UR) to govern the design of ice-class and polar-class vessels (IACS, 2016). These use a plastic limit state for ship structural design as opposed to the traditional elastic design used for most other ship types. The polar rules, however, do not specify requirements for the connections between rule-defined shell plating and framing and the deeper supporting structure. The current design being used for these connections often includes completely welded collar around each intersection between transverse framing and longitudinal stringers. While structurally effective, this design increases weight by using additional steel as collars are labour-intensive, and therefore very costly. This introduces a desire for a more cost-effective design that provides the required structural support.

Four connection designs were subjected to the IACS UR I2 structural requirements design ice load: a fully welded case to represent current practices a baseline for comparison; a full slot penetration with no welding between the stringer and stiffeners; an edge weld case where one side of the penetrating stiffener is welded to the stringer; and an edge weld case with a lug added to the open side to increase strength. To analyze the response of the stiffening structure and the surrounding plating, non-linear finite element analysis (FEA) models were created. The connection designs were checked under four different load

position scenarios: ‘Design Waterline’, ‘Centred on the Stringer’, ‘Centred Between Stringers’, and ‘Edge of the Stringer’. The resultant displacement, effective plastic strain, and stress profiles were analyzed under the design load and for the residual deformation after the loading event to form conclusions about the structural adequacy of the connections. From these analyses, alternative cost-effective connection designs have been proposed for ice-class vessels that use less steel while maintaining an acceptable structural response.

This thesis contains five chapters with each containing various sub-sections. This chapter, chapter 1, is the introductory chapter that includes the scope of this paper and background information discussing the current polar class rules, FEA and the finite element method, and information regarding current practices. Chapter 2 is a review of the literature studied in the process of writing this thesis. Chapter 3 describes the methodology behind both the three-dimensional models created and the FEA models. Chapter 4 summarizes the results from the simulations and what they mean. Finally, chapter 5 explains the conclusions gathered from this project and gives recommendations for future ice-class builds.

Chapter 2 Literature Review

Not much prior research has been done into the connection region between main ice strengthened structure. In the past, ship structures have largely been designed around an elastic design point. As the design load increases, then the structure must be redesigned to remain elastic. As mentioned, current unified rules allow for a small amount of plasticity in large members (IACS, 2016) as a plastic failure point. One of the main reasons that

plasticity was chosen to be a design point in the polar rules was to ensure that there was a degree of overload capacity (Daley & Kendrick, 2002). Unlike hull plating and framing, large structural members are not covered by the IACS UR2 Polar Class rules. Because of this, classification societies are free to choose a design point for such members. Normally, an elastic design point is chosen. Since transitions or connections are currently required by classification societies, primary structures in ice-class vessels must be extremely robust to ensure they stay elastic. The strength effects of transitions from the plating and frames to the primary structure is not something that is fully understood on ice-class vessels. This opens up the opportunity for research that could lead to improvements to current designs, and ways to cut costs in the construction of said vessels.

Cost of construction is an inspiration for the research done in this thesis. Penetrations (also known as “cutouts”) can be cut into large stringers during the manufacturing process. The excess steel from these cuts can then be recycled and used for other purposes such as for recycled parts in automotive, aircraft, or shipbuilding production. Eliminating some level of welding from the ship construction process can also drastically reduce cost (Leal & Gordo, 2017). While a detailed cost-benefit analysis was not performed, it is assumed that simpler structural layouts with less total weld length are cheaper to produce. Welding personnel, weld area, and hours required are all multiplicative factors that go into the total cost of shipbuilding. With the design of a fully welded collar around certain stiffener-stringer intersections, welders must enter cramped spaces with no access to the underside of the stiffener from the top side and must complete a full weld around the intersection between the two structural members. With larger penetrations that do not require welds

around the entire intersection area, the man-power required, the weld area, and welding time is drastically reduced resulting in far lower costs for the ship manufacturer. According to Leal & Gordo (2017), costs and time spent welding on large panels with large reinforcing structures are much greater than other areas such as bulkhead unions.

Some general research has been done into reducing and optimizing polar class vessel construction costs. As Normore (2007) outlines, there are two main methods of cost estimation, the Systems-Oriented Work Breakdown Structure (SWBS) and the Product-Oriented Work Breakdown Structure (PWBS). In general, a SWBS outlines the set of tasks that need to be completed throughout the project while a PWBS outlines the deliverables to be completed. In North America, it was more common to see a SWBS used instead of a PWBS. This cost estimating method is based heavily on ship weight, material cost per tonne, and production cost per tonne (Normore, 2007). The production cost per tonne is influenced by the difficulty of constructing the vessel in a certain region. This production cost depends heavily on shipyard labour costs (Miroyannis, 2005). In some cases, an estimate of half of the total ship construction cost can be assumed to come from shipyard labour (Ross, 2004). Normore (2007) outlines that shipyard labour costs are driven by:

- Thickness of material being joined by a weld
- Number of weld passes required
- Material grade
- Accessibility

Normore (2007) recommended that “Polar Class 1 and 2 should be designed analyzing both weight minimization and cost production minimization methods to develop a better understanding of the design space to determine the most efficient design.”

2.1 Finite Element Analysis Modeling

Successfully performing non-linear FEA involves many specific model inputs to ensure accuracy of the results. Even small errors in inputs can result in an entire simulation being invalid. Element type is an important consideration. When modeling any area of the hull, or any ship structure that is larger in two dimensions than a third dimension, shell elements with a minimum of five (5) through thickness points is recommended (LSTC, 2022). In linear elastic FEA, a common practice is to use beam elements to model stiffeners, however in non-linear FEA (especially in regions of highly non-linear behaviour such as the ice belt), it is strongly recommended to use exclusively shell elements to model stringers and stiffeners. Beam elements are not able to accurately capture the changes in the cross-sectional shape of the stiffener since the cross section of a beam element is not physically part of the geometry and is simply a parameter (LSTC, 2022). Further discussion of element type and formulation is done in Section3.4.

Determining proper element size in non-linear FEA is necessary to find the correct balance between computational efficiency and accurate results. Element size for non-linear FEA should always be determined from a mesh convergence analysis. As element number increases, the physical response of the structure is better represented as bending or other out of plane behaviour is better captured. There is a number of elements where the accuracy

of the response does not significantly increase with an increase in total elements. At this point, it is beneficial to use the element size that corresponds with this critical number of elements (Quinton et al., 2016). When choosing element size, one must also ensure that the ratio of element size to thickness is appropriate. Typically, it is not desirable to have elements with a side length to thickness ratio of less than 1.2:1 (LSTC, 2022). A further discussion of element size and mesh convergence analysis takes place in Section 3.5.

Boundary conditions are another important consideration when creating an FE model. Previous literature including Daley et al. (2005) state to mimic real world conditions as close as possible when selecting boundaries. This requires the user to set fixed boundary conditions in natural areas where the neighbouring structure to the boundary conditions is sufficiently rigid to consider the boundary nodes as fixed.

One important consideration when performing non-linear FEA, or FEA of any kind, is whether to use an implicit or explicit solver. The choice of implicit vs explicit depends on the problem type. Explicit time integration is typically suggested for solving transient dynamic problems, and is sometimes used to solve highly non-linear quasi-static FEA, or FEA with elastic or plastic instabilities (Quinton et al., 2016). To properly capture highly non-linear behaviour, very small time steps are needed. A maximum stable time step can be automatically determined and solutions are created at each of these intervals. Implicit solvers are much less computationally efficient at producing results for these small time steps when compared to explicit solvers. Static problems, such as the problem presented in this thesis, time is not required for an accurate solution. For these problems, an implicit static solver can be used. Time integration can be included with an implicit solver by using

an algorithm called the Newmark-Beta method, but it was not deemed to be necessary to include for the work presented in this thesis. Automatic sub-stepping can be used to calculate the appropriate fraction of the total applied load at each step until the termination time is reached and the full load is applied. A further discussion of these time integration methods and which was chosen for this research is presented in Section 3.8.

The way the load is applied to the structure can impact the results significantly. The design load magnitude and dimensions were determined from the IACS UR Section I. These rules are discussed in Section 2.3 while the load patch calculations themselves are found in Section 3.11. The process of applying this load correctly using FEA required more research. Daley et al. (2016) stated that when applying a design ice load to a structure, a rectangular patch load is most commonly used with a uniform pressure being applied over it. The simplest way to do this is to select the load patch area within LS-Dyna (or the chosen FEA software) and apply a uniform pressure over all elements (Daley et al., 2016). This uniform pressure is to be applied using a uniform load curve that gradually increases from zero to the maximum load over the course of a small time period.

2.2 Connection Designs

The connection regions on ice strengthened ships at the moment typically use fully welded collars where the transverse stiffeners intersect the longitudinal stringers. However, most ships use various different cutout designs throughout the rest of the vessel. These include designs such as slot cutouts, cutouts welded on one side of the penetrating stiffener or stringer, and occasionally a cutout welded on one side with a

supporting welded lug on the other. Each has their benefits and drawbacks. The Finnish-Swedish Ice Class Rules guidelines for the Structural Design and Engine Output Required of Ships for Navigation in Ice (2017) state that a frame running through supporting structure is to be connected to said structure by either a full collar weld or with a plate or lug of the same thickness of the web plate. This partially served as inspiration for a welded one side with a supporting lug connection design in this research. A slot penetration, while not mentioned as an option in the Finnish-Swedish Ice Class rules, would save the most in costs as there is no welding to be done around the transverse stiffener. A cutout welded on one side provides better strength against an ice load, but stress concentrations, specifically near the root of the web stiffener can become large (Okada & Kawamura, 2018). A weld on one side of the penetration with a supporting lug or tab had potential to be more effective than a slot penetration at distributing the ice load to other structural members and may provide the most structural rigidity of all options presented.

2.3 Rulesets

As more research has been performed regarding ship structural responses in ice, a set of Unified Polar Rules were developed by making a strong effort to combine the polar rules of various countries and classification societies whose ships traveled in icy waters (IACS, 2016). The IACS Unified Polar Rules (2016) were released in 2007 and they govern the design, construction, and operation of all ships that intend to perform "…independent navigation in ice-infested polar waters." (IACS, 2016). These rules give particular minimum scantlings for vessels with a "Polar Class" notation. The different polar classes

each have differing structural and mechanical standards that they must adhere to. Polar class (PC) 1 (the highest polar class) to PC 7 (the lowest) are shown in Table 2-1.

Table 2-1: Polar Class Descriptions (IACS, 2016)

Polar Class	Ice descriptions (based on WMO Sea Ice Nomenclature)
PC 1	Year-round operation in all polar waters
PC 2	Year-round operation in moderate multi-year ice conditions
PC 3	Year-round operation in second-year ice which may include multi-year ice inclusions.
PC 4	Year-round operation in thick first-year ice which may include old ice inclusions
PC 5	Year-round operation in medium first-year ice which may include old ice inclusions
PC 6	Summer/autumn operation in medium first-year ice which may include old ice inclusions
PC 7	Summer/autumn operation in thin first-year ice which may include old ice inclusions

The vessel model in this thesis is a PC 2 as it was designed for year-round operation in moderate multi-year ice conditions. This designation determined the load patch to be used as the design ice load. These rules define the design load for bow and non-bow regions of the vessel and have various multipliers for the design load dimensions and magnitude based on the location that the load is applied on the vessel, and the polar class of the vessel.

2.4 Previous Work

Finite element analysis of ice strengthened vessels has been performed since as early as Hakala (1980) who studied non-linear behaviour of an ice-strengthened ship shell and

compared the results to existing plastic design formulae and experimental results. Other past research has shown that penetrations made directly in way of the load that is applied to the structure results in the stress concentrating around the penetrations themselves (Moakler, 2018). It was also discovered that, in areas that contribute significantly to ice strength, the out of plane displacement can lead to structural failure and thus must be examined. This study also showed the significant effects that supporting tabs on the penetrations had on the overall stiffness of the structure (Moakler, 2018). The tabs increased the overall load capacity and allowed the load to be transferred away from the penetration itself and into the surrounding structure and web frame (Moakler, 2018).

The structural performance of ice-strengthened ships has been studied to some extent with some work on overload performance of such vessels being done by Korgesaar et al. (2018). This work studied ice-strengthened frames under overload cases with varying load patch widths and heights. It was found that in an overload case, the dimensions of the load patch had a significant effect on the ship frames' structural responses. Notably, it was also found that while the response in the structure remained in the elastic range, the ship frames bore most of the load. It was only when the response became non-linear (in the plastic range) that the response shifted more into the membrane stresses of the plating. Finally, it was noted that plastic strain began to localize far faster in ship framing than in the shell plating, and failure maps were developed to show the areas most vulnerable to high plastic strain in their structure. In most cases, as mentioned, frames under the various load patch designs reached fracture strain far faster than the plating,

and the curve relating strain with resultant displacement was far steeper for most frames when compared with plating.

Different designs for ship frames and extra stiffening of these ship frames were mentioned as areas for future research to expand on the findings (Korgesaar et al., 2018). While this thesis only briefly touches on overload cases, the 3-D models, meshes, and FEA models created of an ice-strengthened structure of a PC 2 vessel could be used at the very least as a guideline into future overload case studies.

Bond and Kennedy (1998) investigated post-yield behaviour of a large panel representative of the midbody icebelt region of a Canadian Arctic Class ship by using large indenters to simulate an ice impact. The results obtained were then compared to a non-linear finite element analysis model. They found that non-linear finite element analysis could be used to accurately predict the post-yield behaviour and stability of the ice belt structure in an icebreaker.

Non-linear finite element analysis simulations on ships undergoing an ice load have also been performed, notably by Wang et al. (2008) They investigated the effects of ice loading on an LNG hull by applying a quasi-static ice load to a local side model of an LNG ship hull structure. 5 different load locations (centred on plate, longitudinal stiffener, stringer, web frame, and web frame with stringer) were chosen to best observe the effects on all important structural members. These load locations allowed for the researchers to observe the cases for maximum bending and maximum shear, while also observing the stress and displacement patterns. They state that in the case of static ice loads, such as a patch load,

there is no need to create a large global model and a localized model with adequate boundary conditions is the most beneficial. It should also be noted that shell elements were used to all shell plating and longitudinal stringers in the region of the load patch on this model.

Similar work has also been done by Pearson et al (2015) as they discussed how characteristic stiffness curves could be used to improve structural design in the ice-strengthened regions of polar class ships. They explored the characteristic stiffness curves of seven (7) polar class structures under 150% of the design ice load. To perform these studies, Pearson et al. used LS-Dyna as their preferred FEA software. The entire models of the polar class grillages were created using shell elements and included all cutouts, all stringers, all stiffeners, and any relevant tripping and strength brackets. A mesh size of 50mm was used in their study, however no mesh convergence analysis was presented.

Upon performing their simulations, it was observed that the implicit solver used gave them some problems. At higher loads, such as the 150% design load used in their research, LS-Dyna's implicit solver began to run into issues with convergence of results causing longer simulation times. As Moakler (2018) and Quinton (2016) mention, an explicit solver may be used for highly non-linear cases such as overload cases as implicit solvers have convergence issues, largely due to the structure deforming quickly once the structure goes into the plastic range. Explicit solvers can often capture this rapid behaviour with short time steps while implicit solvers take far longer to compute the behaviour because of the stiffness matrices inverted at each step and the need to iterate over again if divergence in results is found.

Pearson et al. (2015) proposed a guideline that the plastic strain in the ice-strengthened region of a polar class vessel should not exceed 2.5% prior to reaching 150% of the design ice load. This design point, however, has flaws. Plastic strain as a design criterion can be beneficial as it is easily calculated within FEA software and does provide meaningful context as to where plasticity is observed in the structure and to what degree of plasticity exists. The problem lies within how the strain is calculated. In FEA the responses are calculated as an average over each element. Responses such as stress and strain can sometimes vary with a change in element area. For structures with stress concentrations, it may be possible to resolve the peak stresses via mesh refinement, and then the stress will not change with smaller element size. Structures with geometric discontinuities like corners have essentially infinite stress at the discontinuity, and therefore using smaller elements will always resolve higher stresses and strains. Since effective plastic strain could change with mesh size, issues could arise in areas with degenerate elements such as around the penetrations to be studied in this thesis. This criterion is discussed further in Section 3.13.

Chapter 3 Methodology

As mentioned, the goal of this research is to observe the effects that stiffener penetrations have on the structural integrity of the ship's ice belt. The CAD model geometry was made and revised multiple times in Rhino 3D until the model accurately reflected the vessel's structure. The model was then meshed and put into LS PrePost. Once all material properties, shell element thicknesses, boundary conditions, and loads were applied, the model was solved in LS Dyna. After that, iterations were performed to determine adequate

geometric extent of the model, an appropriate mesh size, and to find any potential errors in the model. It should be noted that for this research the effects of welding were not considered. Modeling welds in FEA for ships, especially in a model of this size, is not always common practice. Modeling the weld details can require the use of solid elements which increases modeling and computational time significantly. Modeling the welds themselves are also not trivial as it can be difficult to avoid introducing singularities. Methods to predict weld stresses in FEA exist such as the hot spot stress method, which is well described by Lotsberg (2006), however this method is quite time consuming due to the manual element of hot spot stress calculation. Modeling welds properly increases the overall accuracy of results and is essential in fatigue problems. However, for cases such as this research which focuses on a preliminary assessment of various penetration designs and their influence on the load transfer from an ice pressure, detailed weld modeling was not deemed necessary as the detailed stress profile around the weld area itself was not a driving factor of results.

3.1 Three-Dimensional Model Development

To perform a finite element analysis, geometries for the structures we are concerned with must first be created. Geometries can be made of 0, 1, 2, or 3-dimensional parts. 0-dimensional parts are points, 1-dimensional parts are lines, 2-dimensional parts are planes, and 3-dimensional parts are solids. The models were first developed in Rhinoceros 3D before being imported into Altair HyperMesh for meshing. The geometries for this project were made solely of a combination of 2-dimensional elements known as “shell” elements. This is common practice in shipbuilding and naval architecture, even for stiffeners and

stringers. 1-Dimensional beam elements, while sometimes used in linear analyses, are not appropriate for simulations involving plasticity as the cress sections of such beam elements do not change. For 1D elements, the cross-sectional area is simply a parameter. In simulations involving plasticity, the cross-sectional area cannot change in 1D elements to adequately model the stress and strain within the elements. Because the cross section cannot change shape in response to say web buckling or flange rotation, it cannot capture the stiffener or stringer behaviour during these events. It also requires less computational power to model 2-dimensional elements compared to 3-dimensional elements while maintaining the accuracy of the calculations.

The overall geometric extent of the PC 2 ship model used in the simulations described below was the result of a sensitivity study. Initially, a FE ship model of large geometric extent ranging from the ship centreline to the outer shell with a vertical extent from the ship baseline to the top of the weather deck was subject to the IACS UR I2 design ice load, and the results were observed. The model extent was then iteratively reduced by noting and removing peripheral areas with negligible stress. This process ensured that subsequent FE simulations were computationally efficient while ensuring that the structural response in the areas of interest were not unduly influenced by the proximity of the mesh's boundary conditions. Concurrently, mesh convergence studies were performed to ensure that an adequate mesh size was employed.

The final model consisted of a 6.8-metre-long section of the vessel centred just forward of midship in the region of the icebelt. This includes two web frames spaced 2.4 metres apart, side shell, stiffeners, and longitudinal stringers. The plating, stiffener, and stringer

dimensions were determined from drawings of an existing Polar Class 2 vessel. This model has 21 parts in LS-Dyna. The list of parts and a description of each part is shown in Table 3-1. Note that for part 21, “LOAD” indicates that this part was created separately from the other 24mm DH50 steel layer with the purpose of using this part specifically as the load patch.

Table 3-1: Model Part Numbers and Descriptions

Part No.	Description	Part No.	Description
1	10mm AH36 Steel	12	18mm AH36 Steel
2	11.23mm AH36 Steel	13	18mm AH50 Steel
3	11.5mm AH36 Steel	14	18mm DH50 Steel
4	11.5mm DH36 Steel	15	20mm AH50 Steel
5	12mm AH36 Steel	16	24mm DH50 Steel
6	12mm AH50 Steel	17	6mm AH36 Steel
7	12.35mm AH36 Steel	18	7mm AH36 Steel
8	13.68mm AH36 Steel	19	8mm AH36 Steel
9	14mm AH36 Steel	20	9mm AH36 Steel
10	15.45mm AH36 Steel	21	LOAD 24mm DH50 Steel
11	16mm AH50 Steel		

3.2 Penetration Design

Once the polar class 2 structure was created, the penetrations needed to be incorporated into the model. The penetration designs were determined from a combination of typical

designs from industry experience and suggestions from project partners. As mentioned, the four designs were a fully welded collar, a full slot penetration, a one-sided weld penetration, and a one-sided weld penetration with a tab. Figure 3-1 through Figure 3-11 show isometric and plan views of the CAD geometry models for each penetration design, plus the same views for the fully welded collar case.

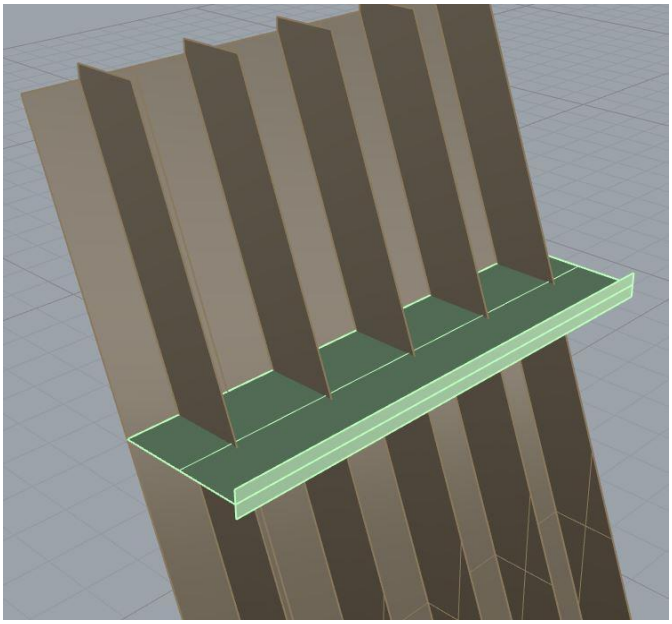

Figure 3-1: Fully Welded Connection - Isometric View

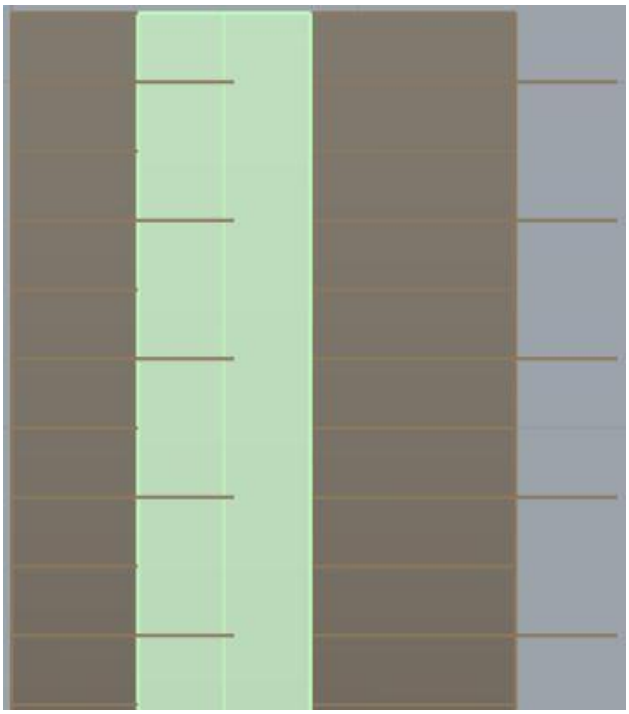

Figure 3-2: Fully Welded Connection - Top View

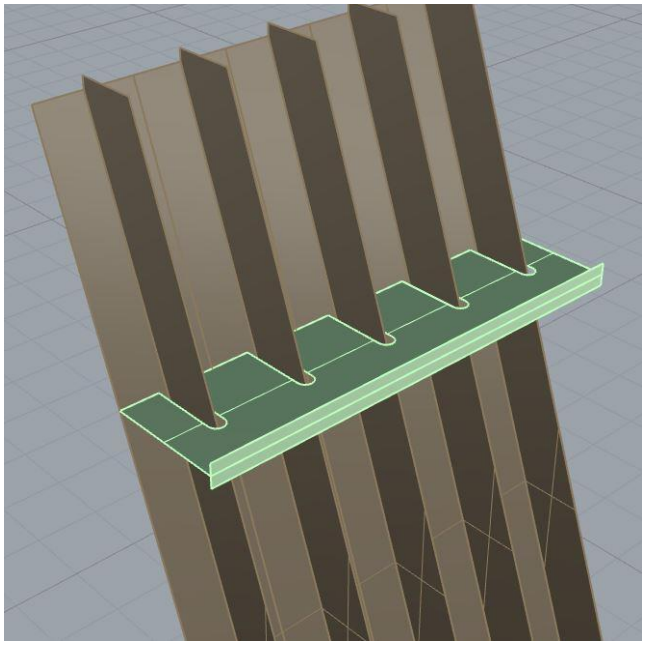

Figure 3-3: Slot Connection - Isometric View

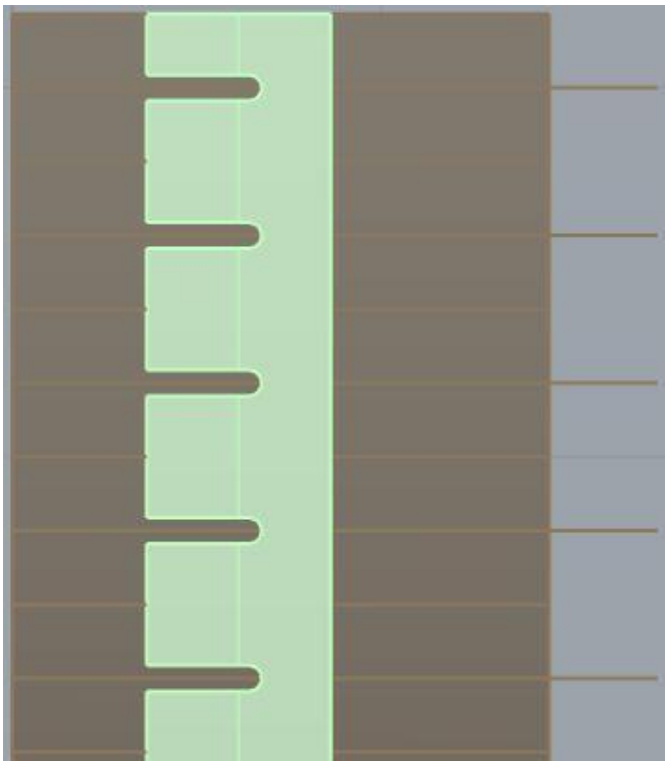

Figure 3-4: Slot Connection - Top View

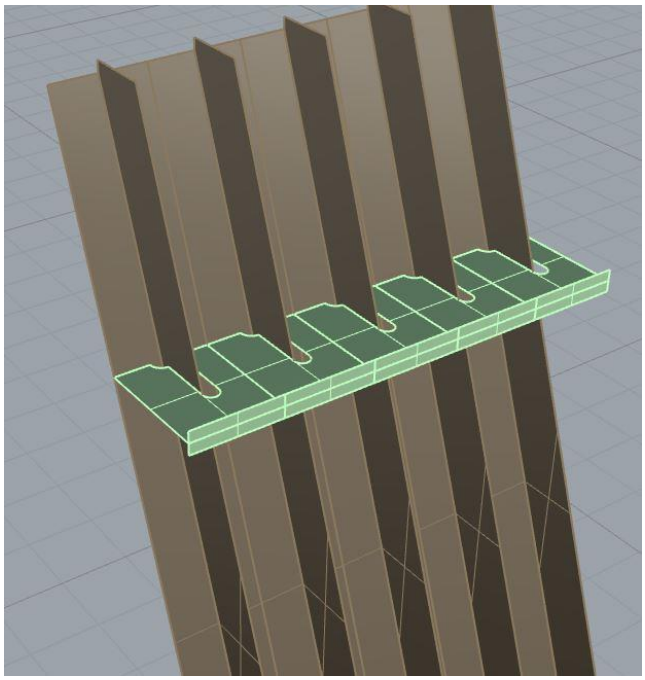

Figure 3-5: Welded One Side Connection - Isometric View

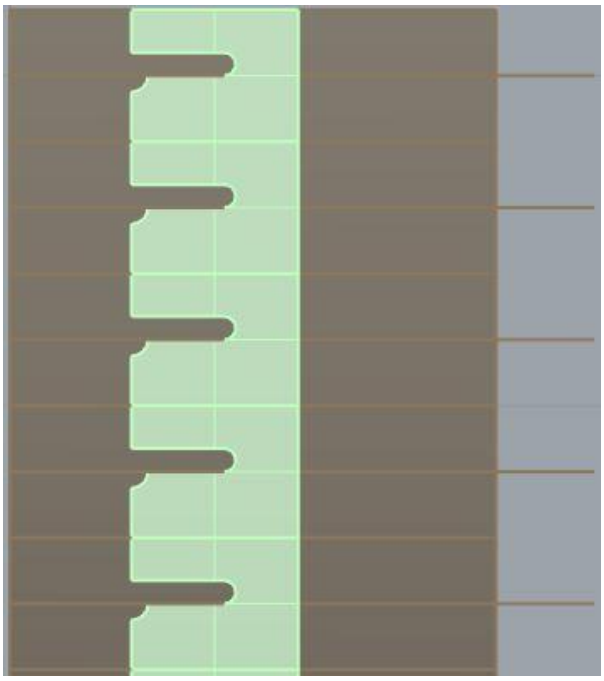

Figure 3-6: Welded One Side Connection - Top View

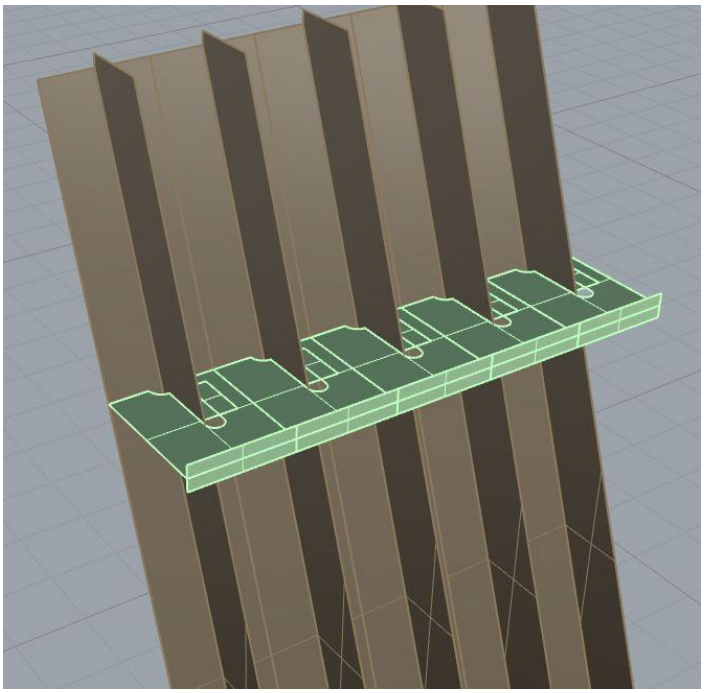

Figure 3-7: Tab Connection - Isometric View

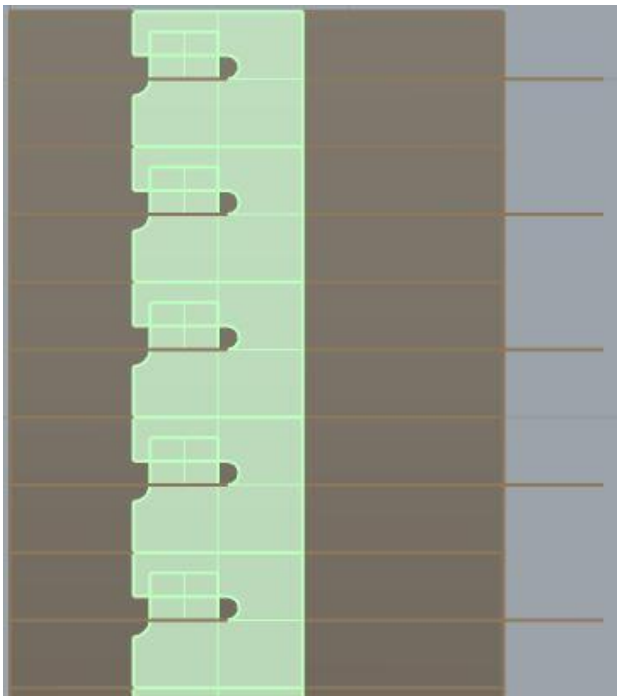

Figure 3-8: Tab Connection - Top View

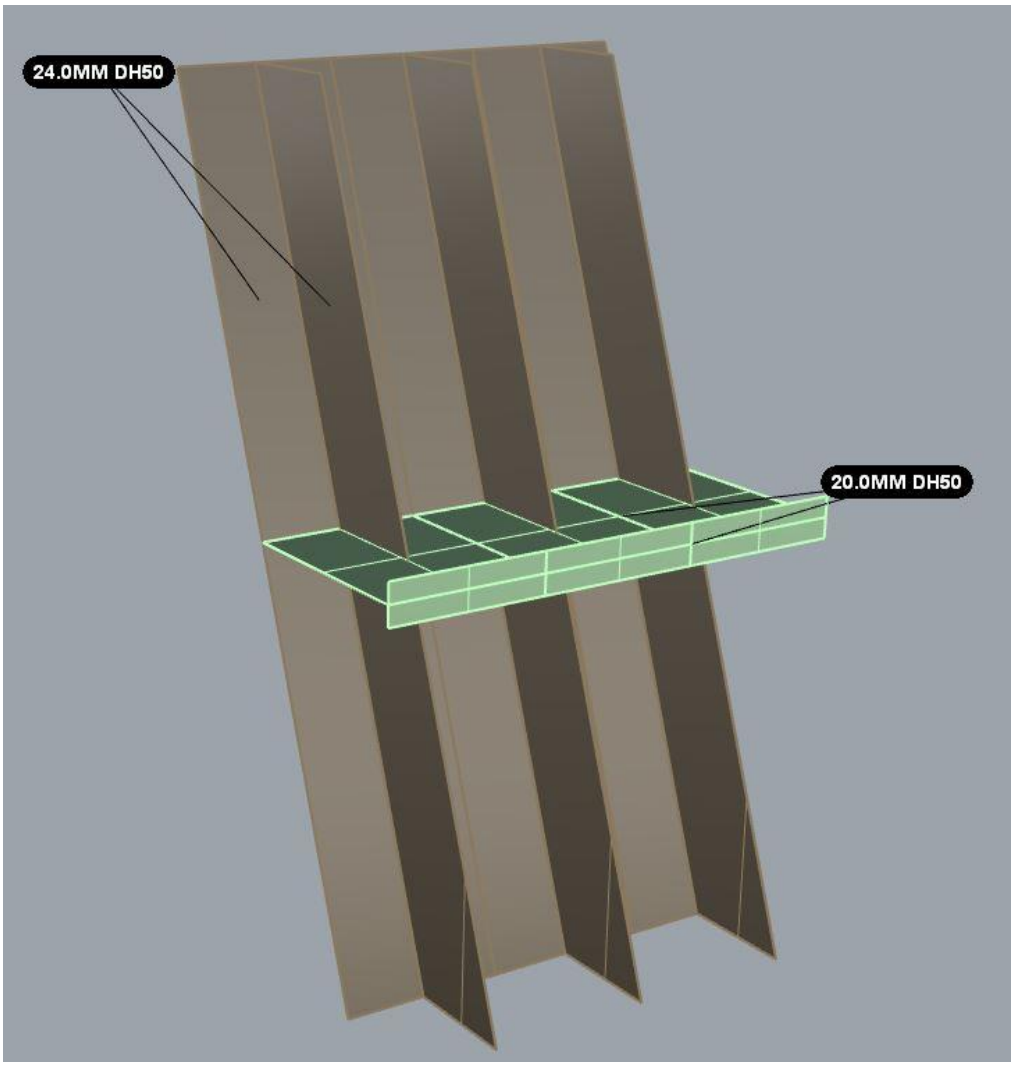

Figure 3-9: Penetration Design Specifics - Isometric View

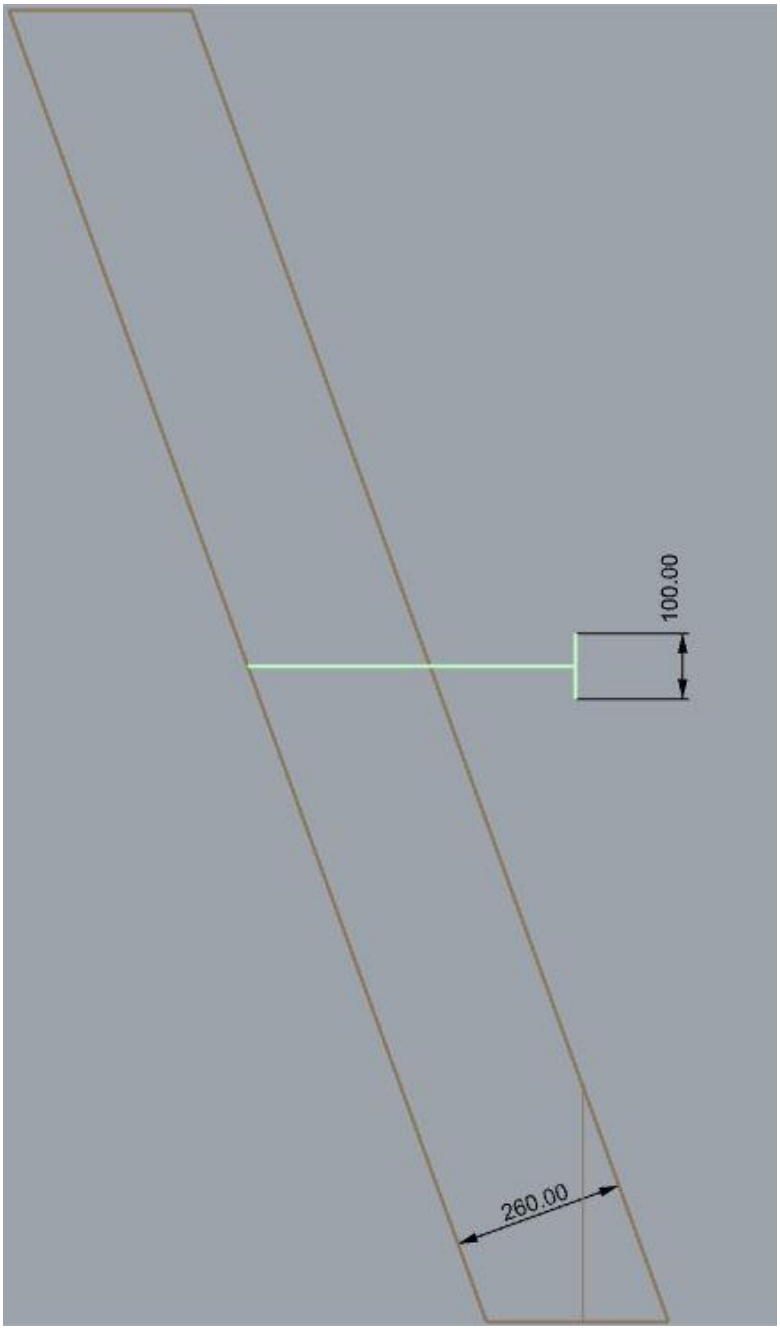

Figure 3-10: Penetration Design Specifics - Profile View

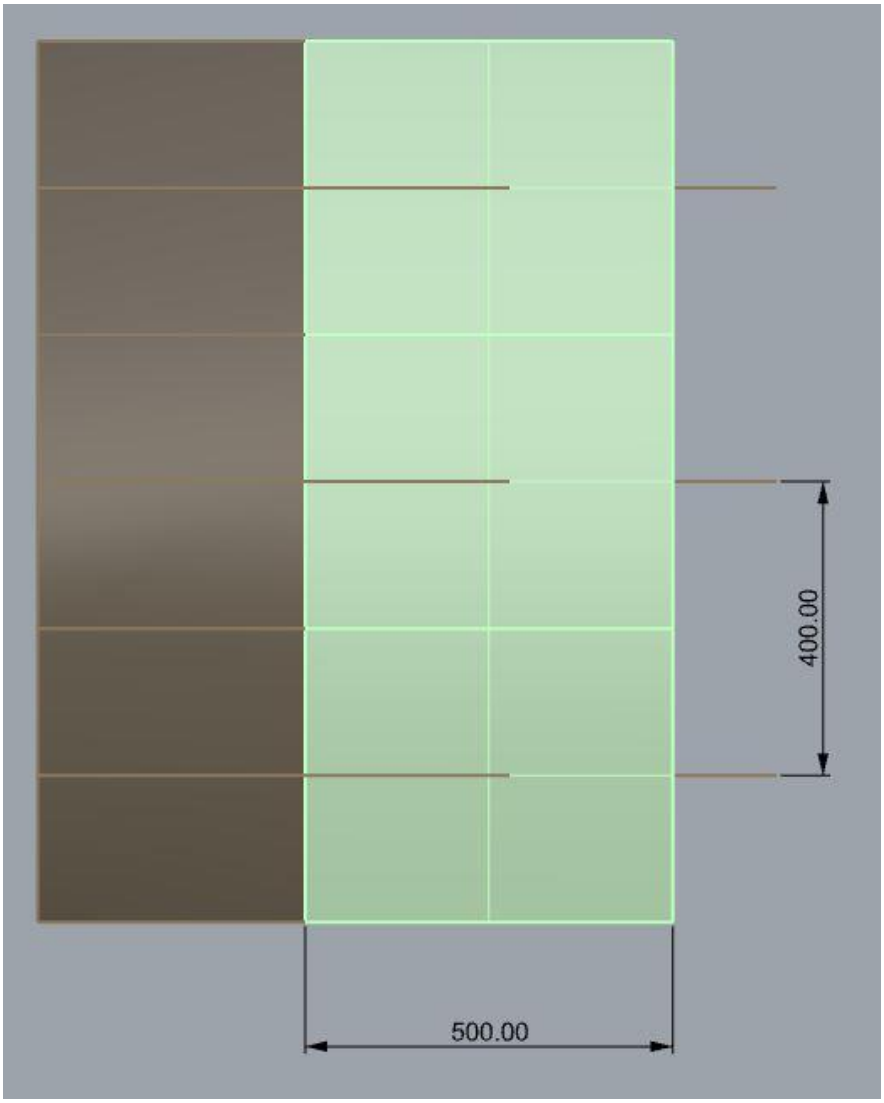

Figure 3-11: Penetration Design Specifics - Plan View

3.3 Linearity in FEA

When preparing a finite element analysis model and deciding upon a solver, the linearity of the model must be considered. The model may be linear or non-linear. In models with very small expected deflections and linear material properties, a linear solver can be used. However, if any non-linearities are present a non-linear solver must be used. Non-linearities can be found in various parts of a FEA model and exist in three forms: geometric,

material, and boundary non-linearities. Geometric non-linearities often stem from an applied load causing large deformations as the material may no longer follow a linear relationship with the strain curve. Any modeling of the plastic region of a material is considered a material non-linearity as the stress-strain curve is no longer in the linear-elastic region. A boundary non-linearity can occur at occur because of poor mesh quality that leads to detached elements or nodes. Non-linearities increase the simulation time of a model as the equations that need to be solved at each step become more complex when compared to a linear elastic model. This is amplified when using implicit solvers as each time step becomes much more computationally intensive to reach convergence because iteration is necessary.

3.4 Element Type

Every element modeled throughout this project was a shell element. Shell elements are very well-suited for modeling the steel plating and supporting structure of a ship. In general, if an object is much smaller in one dimension than the other two dimensions, a shell element is the ideal choice. All objects in this project had dimensions suitable for modelling with shells. When defining said shell elements within the *SECTION_SHELL card of LS-PrePost, there are various user inputs that affect the results of the simulations. Notably, the shear correction factor and number of through thickness integration points should be defined by the user.

Shear correction factor scales the transverse shear stress for an element. This is because shells in LS-Dyna use first order shear deformation theory, that does not account for second

order effects (LSTC, 2022). The shell elements used were all isotropic and homogeneous with a rectangular cross section, so a shear correction factor of 5/6 ($0.8\overline{33}$) (LSTC, 2022) was applied across all cards.

Shell elements in LS-Dyna have no thickness and are just planes. Without a thickness, there can be no bending response. To counteract this, the user defines a thickness for each shell element along with a number of through thickness integration points. Through-thickness integration points are the location where through-thickness stresses are calculated. This ensures that LS-Dyna can accurately account for the changes in responses such as stress and strain throughout the thickness of the element. For non-linear shell elements, a minimum of three through thickness integration points should be used (LSTC, 2022). However, for thick elements and for nonlinear behaviour, five through thickness integration points improves accuracy (LSTC, 2022). All shell elements in this project were given five through thickness integration points to improve the accuracy of the results.

There are multiple choices of formulations for the elements in LS-Dyna. The two main element formulations used in LS-Dyna are Belytscho-Tsay (B-T) and Hughes-Liu (H-L). Both are suitable for non-linearities and plasticity in elements, but H-L elements are slightly better than B-T elements for large deformations. Naturally, this also means increased computational costs. For the purposes of this research, exceedingly large plastic deformations are not expected, so the more computationally efficient B-T elements were chosen for all simulations. Finally, the choice of element order should be made. The order of the element indicates how many nodes comprise the elements and whether the lines connecting these nodes can represent curvature. All elements in this research are first order

elements indicating that nodes are only at the corners of each element and the lines connecting these nodes are straight. This saves computational resources and the lack of curvature in the elements is compensated for by using smaller elements in general.

3.5 Mesh Convergence

The entire 3D model is discretized into small polygons referred to as “elements”. This discretization is what makes up the mesh. When performing a finite element analysis, a mesh convergence analysis (MCA) is a mandatory step to ensure the results of the model are accurate. As the size of elements in a mesh decrease, the results get more accurate since the model is essentially being analyzed in a higher resolution, but as the elements shrink beyond a certain point, it becomes computationally inefficient to calculate the results. However, if the mesh is too coarse, then the results will not be accurate enough as the mesh is now restricted in the shapes it can make. An MCA involves making a coarse and a fine mesh and observing the results of each. If the results differ between the two meshes, then a finer mesh must be created to then be solved again. Note that when performing an MCA for structures that have geometric discontinuities, one must check something other than the stress or strain results as these are mesh dependent and will change depending on element size. A more appropriate output to use, and the one used in the MCA in this study, is the resultant displacement of the nodes. This process is repeated until further reduction in element size has no noticeable effect on the results of the analysis. This point marks a balance between computational efficiency and accuracy of results.

The first mesh for the MCA used element with an average edge length of 0.05 metres. This mesh was created in HyperMesh and then ran through LS Dyna with appropriate boundary conditions and load magnitude. This process was repeated for meshes with average element edge lengths of 0.04m, 0.03m, and 0.02m. As mentioned, the maximum resultant displacement of the model was used to determine which meshes were appropriate. A plot of maximum resultant displacement versus average element size can be observed in Figure 3-12.

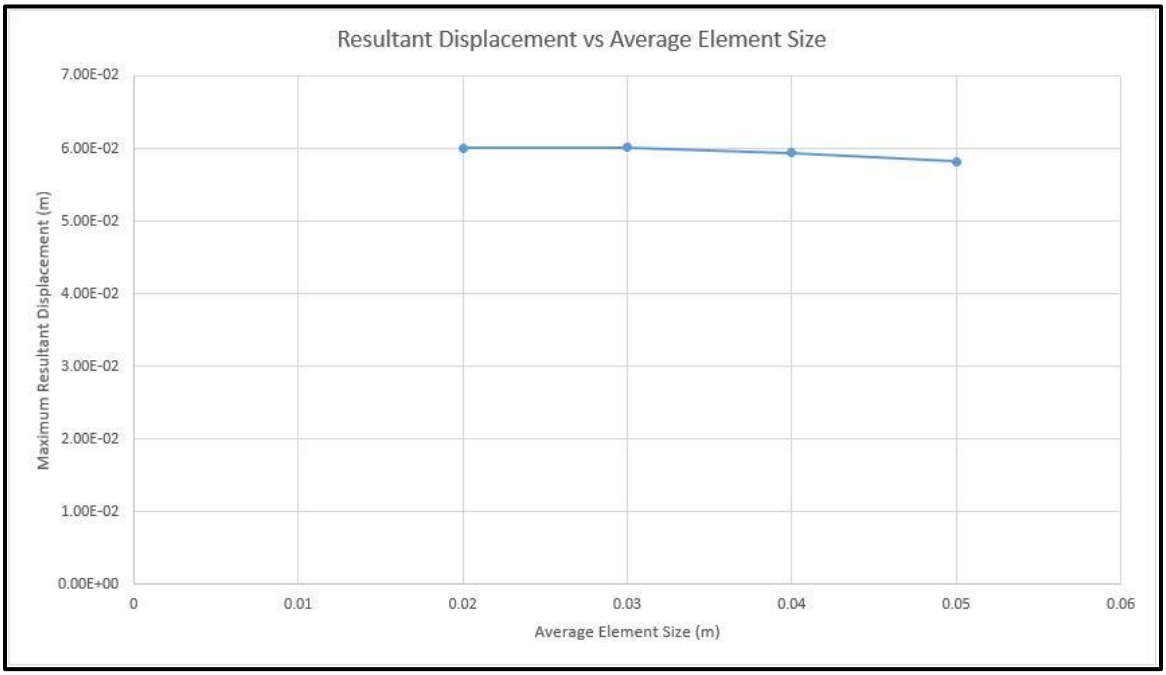

Figure 3-12: Mesh Convergence Analysis Results

Typically, a mesh can be chosen once the difference in resultant displacements between two sizes reaches a value under 5%. As can be observed from Figure 3-12, the resultant displacements do not vary much between runs. The largest difference observed was approximately 2% between the 0.05m mesh and the 0.04m mesh. When computing power

and runtime of models is a large constraint, the largest acceptable element size from the MCA could be chosen. However, since the runtimes of these meshes were very fast, a final mesh size of 0.03m was chosen as this marginally finer mesh did not add a significant amount of real-world simulation time. This mesh is still acceptable based on the results of the MCA as there is no significant difference between the resultant displacements of it and the finest mesh of 0.02m elements, and it also allows for more accurate results.

3.6 Model Development

Within the LS PrePost software, each of the shell elements that make up the ship model must be assigned a thickness and material properties by using the *PART, *MAT, and *SECTION cards. Upon meshing of the model in HyperMesh, the geometry was exported as a .k file that is compatible with LS PrePost. Once the model is brought into LS PrePost, the various parts that make up the model must be properly defined. First, the *MAT cards must be populated. These cards require material properties definitions for Young's modulus, material density, Poisson's ratio, yield strength, and strain-hardening. The specific material models are discussed in depth in Section 3.10, and the *MAT cards are shown in Figure 3-13 and Figure 3-14.

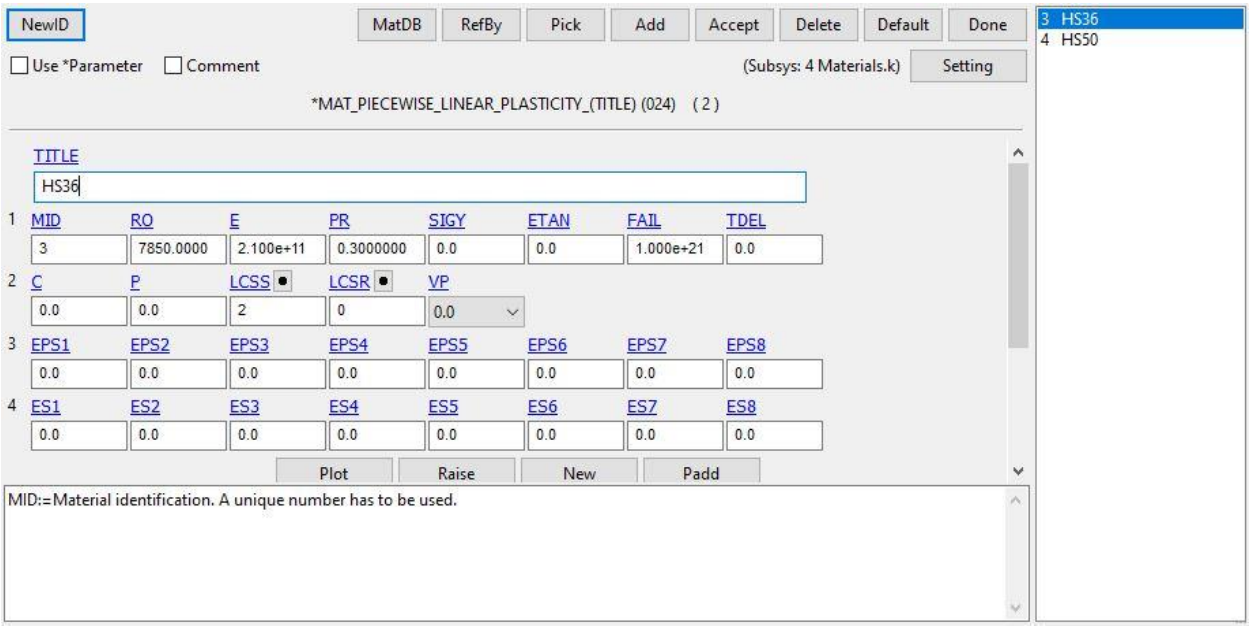

Figure 3-13: *MAT_PIECEWISE_LINEAR_PLASTICITY Card for HS36 Steel

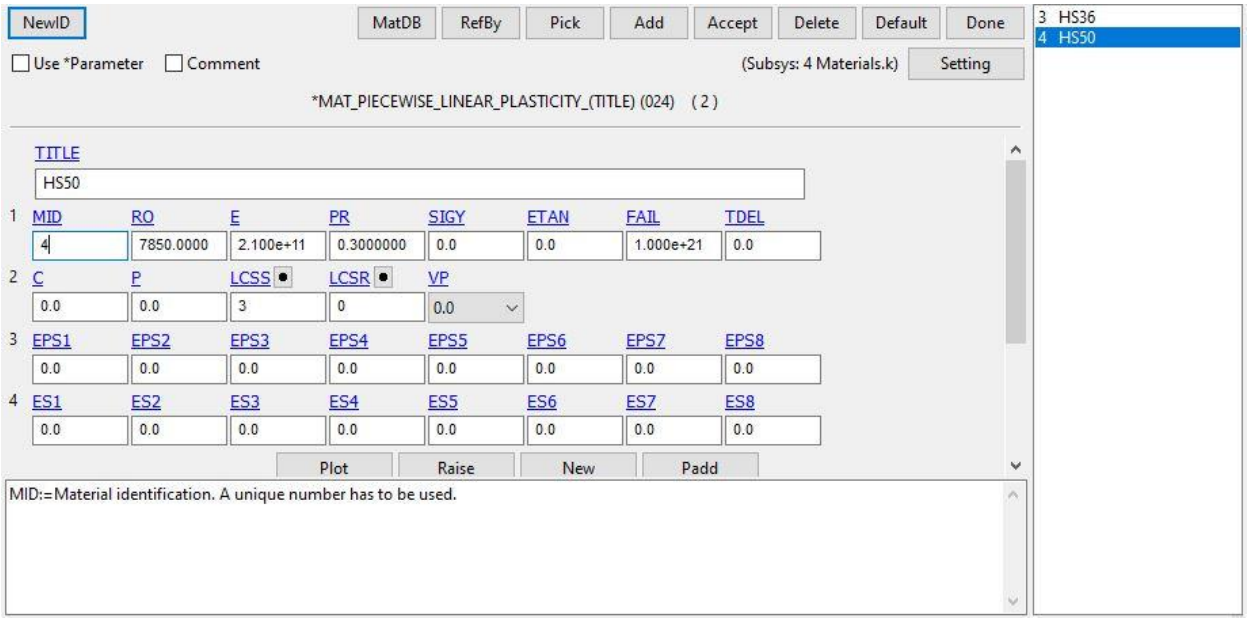

Figure 3-14: *MAT_PIECEWISE_LINEAR_PLASTICITY Card for HS50 Steel

Next, cards to define the various thicknesses for the elements were created. This was done using the *SECTION cards. An example is shown in Figure 3-15. The subsection of "shell"

was selected since all elements in Hypermesh were shell elements. This card requires input for the shear correction factor (SHRF), the number of through thickness integration points (NIP), and the thicknesses at each point of the shell. All other inputs for this card were left unchanged. For simplicity, the thickness is assumed to be constant throughout each shell element.

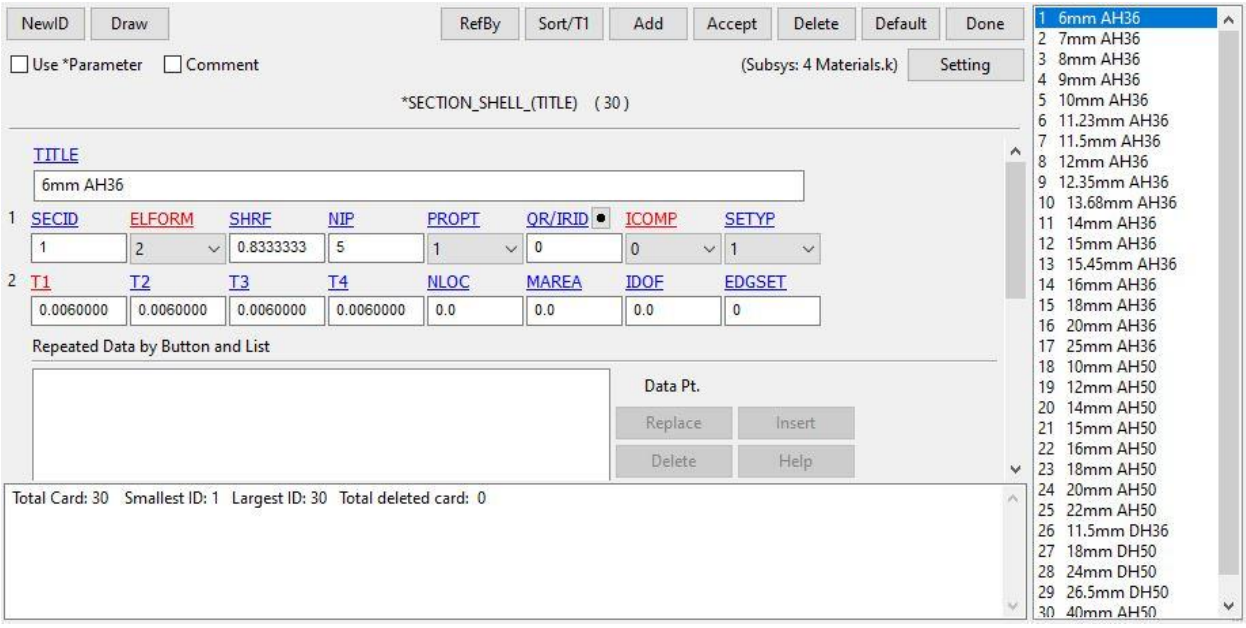

Figure 3-15: *SECTION_SHELL Card for 6mm AH36 Steel

Each separate layer from the CAD model has a corresponding “Part” in LS PrePost. Each layer gets a corresponding *PART card. The *PART card allows for the assignment of the material ID and section ID from the cards created in the two previous subsections. For example, if a layer was for 12mm thick AH36 steel, the *PART card would identify the material ID as AH36 Steel and the section ID of a 12mm thick shell element as shown in Figure 3-16. The various combinations of material and shell thicknesses correspond with the structural drawings of the PC2 ship, which may not be shared in this publication.

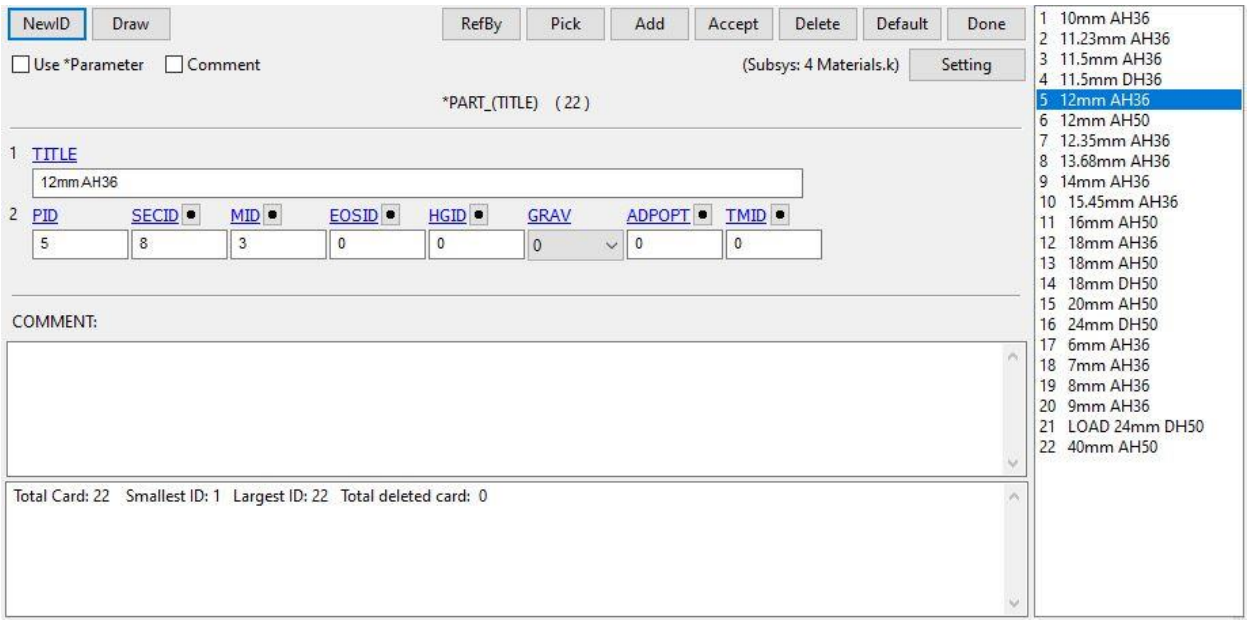

Figure 3-16: *PART Card for 12mm AH36 Steel

3.7 Boundary Conditions

To obtain meaningful results, the meshed model must have appropriate boundary conditions applied. Without boundary conditions fixing the position of certain parts of the model, the model would be free to move through space once a load of some kind is applied. Boundary conditions are applied to nodes within the model that should be restricted in displacement and/or rotation in some way. When selecting the boundary conditions for shell element nodes in LS PrePost, they can be restricted in six possible ways, i.e., shell element nodes have six degrees of freedom (DOF). These DOF are displacements in the x, y, and z directions, and rotations about the x, y, and z axes.

These boundary conditions were applied using the “Create Entity” section of LS PrePost. This feature created two separate cards (*BOUNDARY_SPC_SET and *SET_NODE)

which allowed for one set of single point constraints that included all outside edge free nodes to be created. The rotation and translation restrictions mentioned above were then applied to this node set. Figure 3-17 through Figure 3-20 show various angles of the side shell model with boundary condition nodes highlighted.

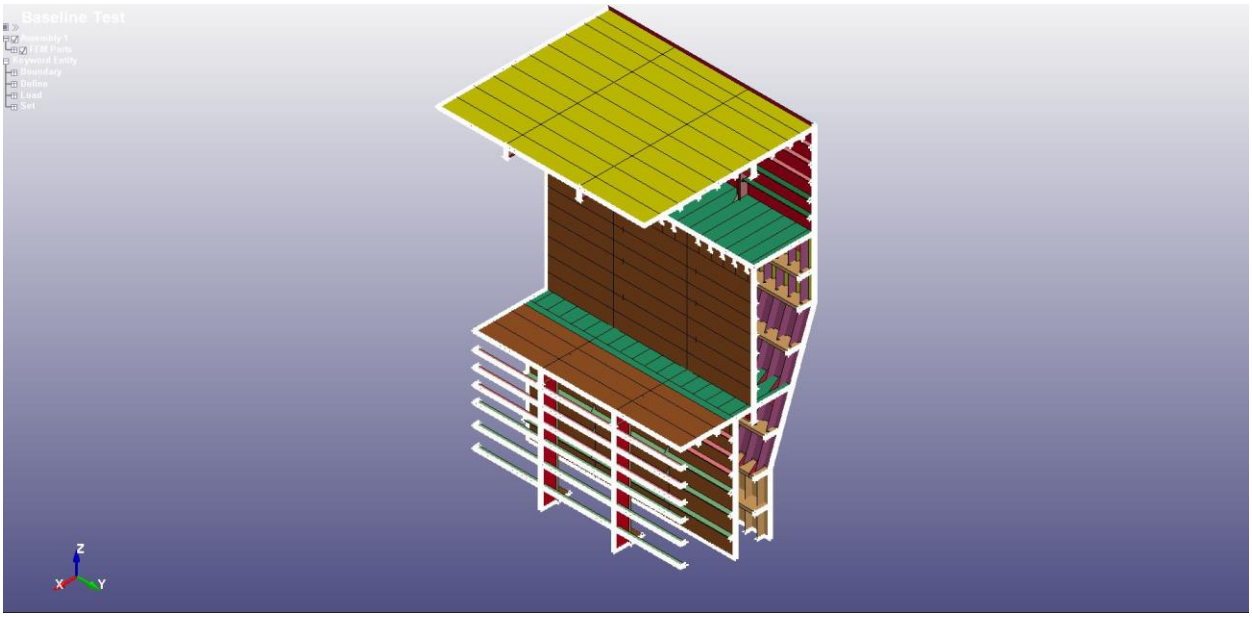

Figure 3-17: Boundary Conditions - Isometric View

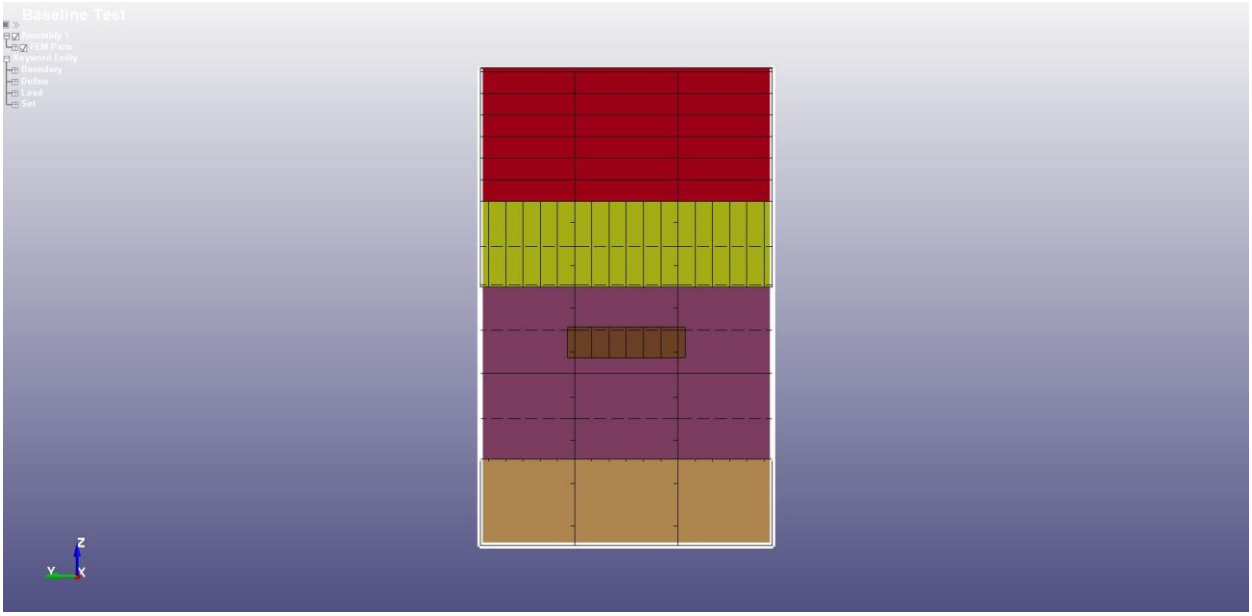

Figure 3-18: Boundary Conditions - Front View

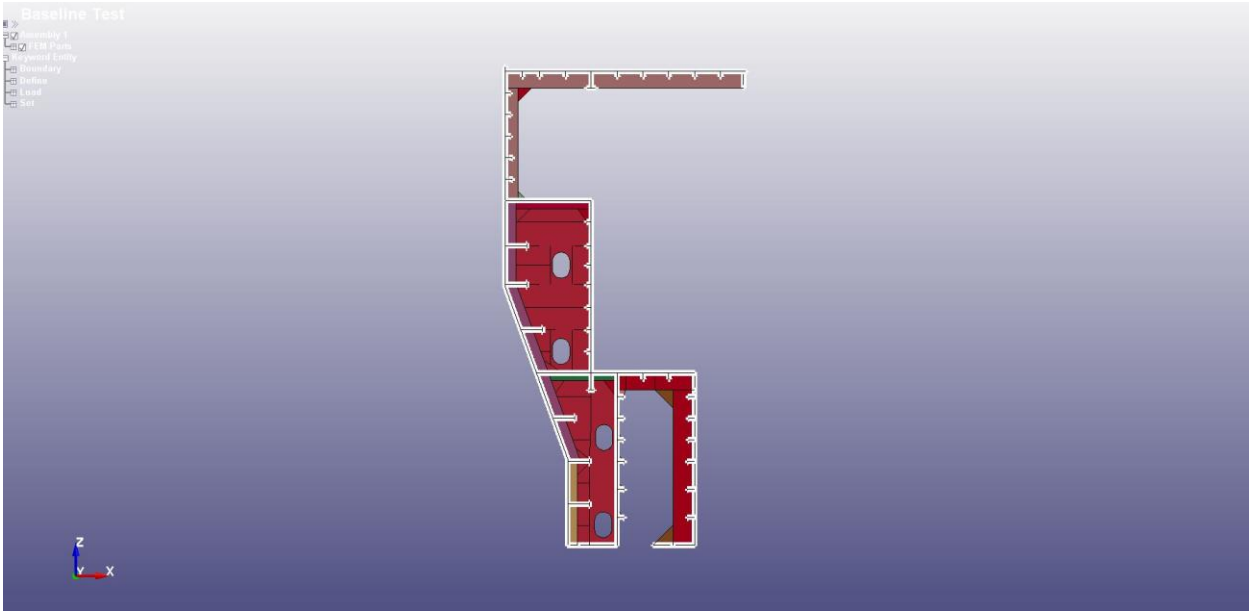

Figure 3-19: Boundary Conditions - Side View

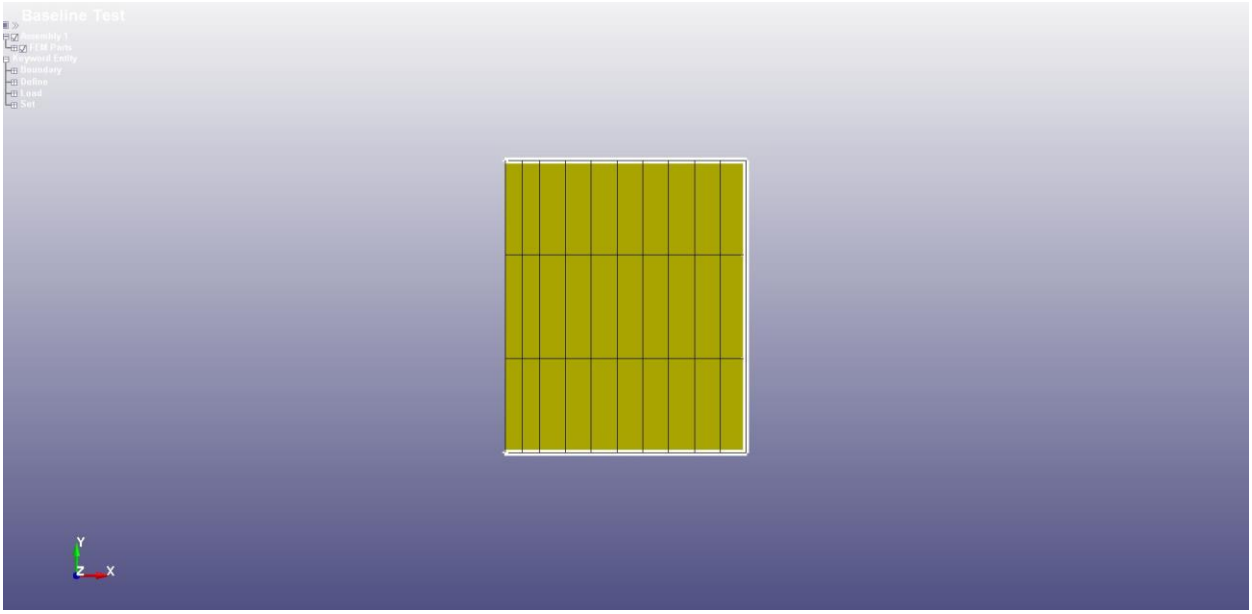

Figure 3-20: Boundary Conditions - Top View

The boundary conditions were chosen at these locations as they are in locations that have large amounts of structure connected to the respective nodes. On the forward and aft side nodes, there is a web frame connected. On the inboard side of the lower part of the model, there is a bulkhead connected. Each node where a stiffener or stringer continues is fixed. Finally, a node was fixed if the deck continued. It was assumed based on the information known of the surrounding structure that in all cases mentioned, the structure was rigid enough to not allow for movement or rotation of any node at the selected boundary conditions, thus each node was fixed in all degrees of freedom. Without these fixed boundary conditions, plating within the model cannot develop membrane stress and stiffeners cannot develop tension. Both of these properties are highly relevant for the analysis of ice class structures.

To ensure the boundary conditions were appropriate and did not alter results, an FEA simulation using this model extent was performed. After this simulation, responses at boundary conditions were checked to ensure no stress or strain concentrations were present that were skewing results. With no significant responses at the boundaries of the model, it was determined that these conditions were adequate.

3.8 Analysis Type – Implicit vs Explicit

FEA software has two main ways of solving problems, explicitly or implicitly. These two methods differ in multiple significant ways and the proper solution method must be chosen to ensure accurate results are obtained.

In implicit analyses, the step can be defined by the user, or it can be automatically generated, and the model gets solved for each step until the desired end time. During each load step, iterations are performed on the model until convergence of results is observed. This represents a "global equilibrium". The necessity of these iterations naturally causes each step in an implicit analysis to solve slower than its explicit counterpart. However, since global equilibrium is confirmed after each increment, these increments can be much larger than explicit increments thus leading to there being fewer total time steps. This helps in problems that may have an end time on the order of multiple seconds.

In an explicit analysis, the time step is not defined by the user. Instead, the solver chooses which time step is appropriate. In these cases, the time step must be extremely small so that the model can exist in equilibrium. For quasi-static problems such as those analyzed in this thesis, this causes each model to require far more time steps than an implicit analysis would

require, for the same termination time. This large increase in required time steps requires significant computing power. This causes explicit analyses to take longer to solve quasi-static problems than implicit analyses of the same duration, however these extremely small time steps may allow explicit analyses to provide more accurate results.

For the purposes of this research, a static implicit solver was used. The load being applied is not a rapid collision, it is a uniform pressure patch being applied over a period of one second, which is a quasi-static problem as any inertial effects are negligible. Since the load is not applied extremely rapidly, there should be no significant effects relating to this research that an explicit analysis would catch over an implicit analysis. If a problem can be solved accurately implicitly, the results from an explicit analysis should be essentially the same. The model was run in both an explicit and implicit solver to check the difference in maximum resultant displacement. Note that the maximum resultant displacement for the implicit solver was 61.01 mm while the maximum resultant displacement for the explicit solver was 62.00 mm. This means displacement results matched to within 0.001 m (1.16% difference), which was deemed acceptable for this study, thus confirming that an implicit solver was the correct choice for all following simulations. These resultant displacement results for both implicit and explicit solvers are shown in Figure 3-21 and Figure 3-22.

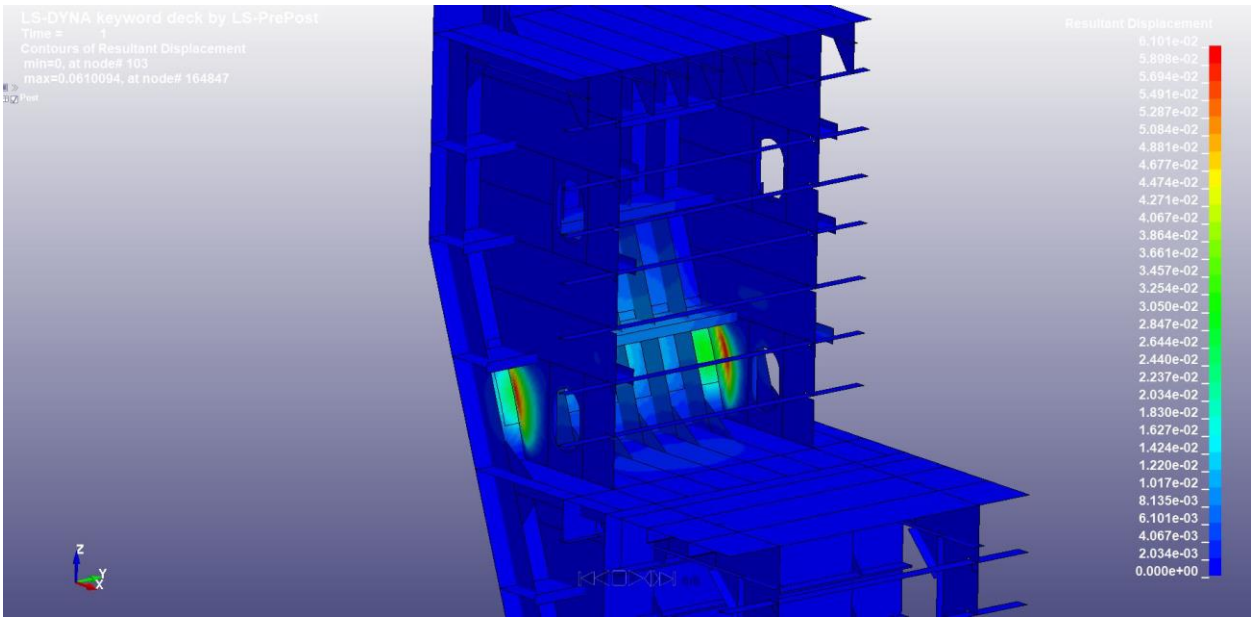

Figure 3-21: Resultant Displacement - Implicit Test

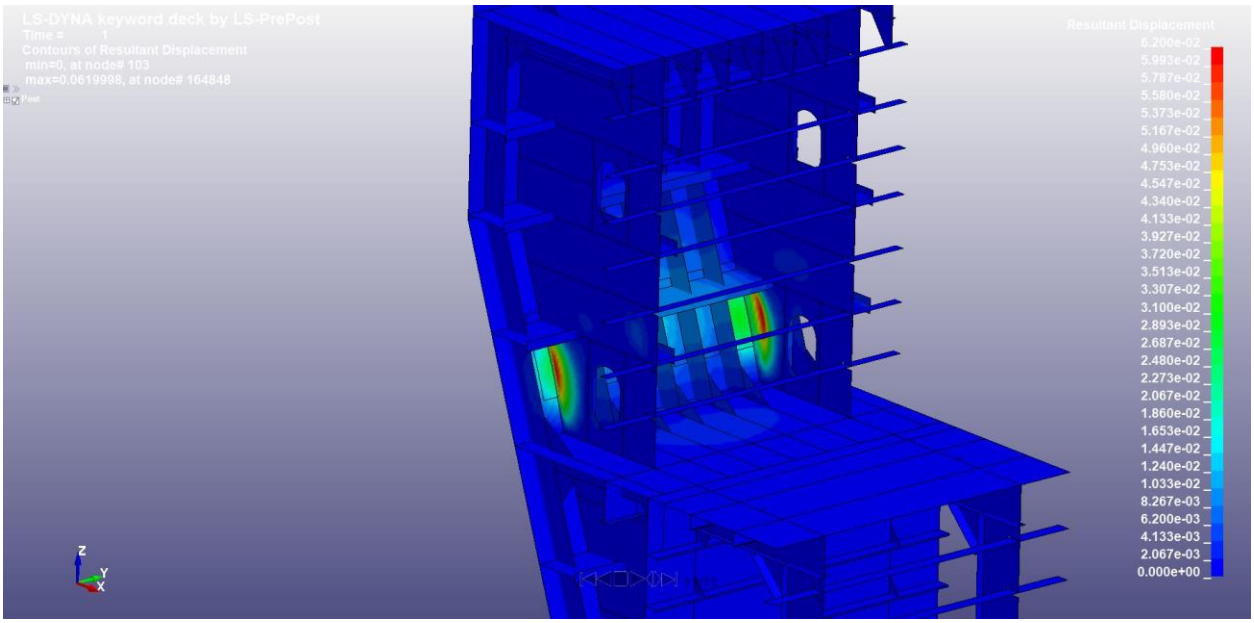

Figure 3-22: Resultant Displacement - Explicit Test

3.9 Implicit Analysis Inputs

In implicit analyses, the user defines the time increment and end time that the solver will use. To define the various properties of the implicit solver, two *CONTROL cards are used. There are the *IMPLICIT_GENERAL and *IMPLICIT_AUTO cards.

*IMPLICIT_GENERAL is a card used to define stepping increments for implicit analyses among other things. For the purposes of this research, only the step section, DT0, is used. For all runs and initial time step is required to be defined by the user. This initial time step was set to 0.1 seconds and was input using DT0. The card is shown in Figure 3-23.

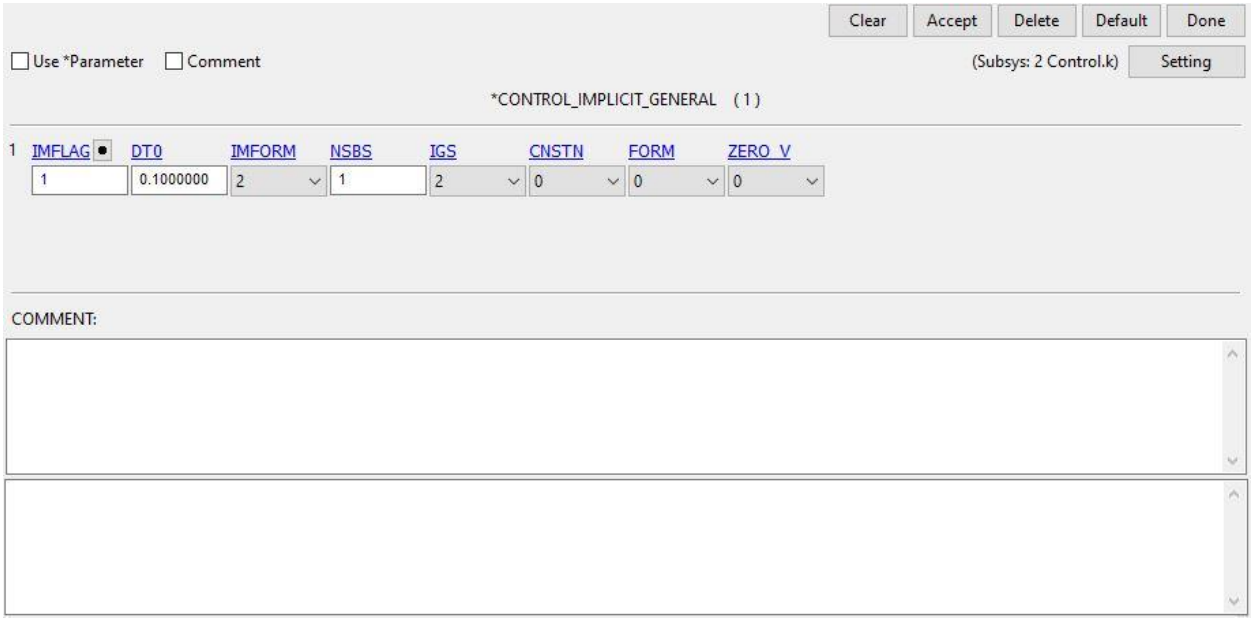

Figure 3-23: *CONTROL_IMPLICIT_GENERAL Card

*IMPLICIT_AUTO allows for the user to choose whether they want the solver to have a constant time step or an automatically chosen time step while also allowing for some control over the optimum iteration count and iteration windows. This card is shown in

Figure 3-24. For most runs, this card was implemented but left unchanged. This allowed LS Dyna to automatically adjust the time step and resulted in a shorter time to reach a solution. LS Dyna was able to solve this model while using only 6 total time steps ending at the one second termination time. To ensure these 6 steps were enough to have accurate results, this *IMPLICIT_AUTO card was deleted for some runs. This forced the model to run with the constant time step defined in the *IMPLICIT_GENERAL card which was 0.1 seconds for all runs. The difference in results between defining a time step and allowing for automatic time stepping was negligible thus confirming that leaving the *IMPLICIT_AUTO card active would be the most efficient choice.

Figure 3-24: *CONTROL_IMPLICIT_AUTO Card

3.10 Material Model

Results for FEA simulations are heavily influenced by the material model. The choice of material model is influenced by the nature of the analysis with a significant factor being whether plasticity is to be considered. In the case of this analysis, the steel in the model is expected to eventually go into the plastic range, so an elastic-plastic model is used. The card used for this was *MAT_024_PIECEWISE_LINEAR_PLASTICITY. There were no material tensile test data available for the steel, so standard values for the corresponding shipbuilding steels were used from the American Bureau of Shipping's (ABS) "Guidelines for the nonlinear finite element analysis of hull response to moving loads on ships and offshore structures" (ABS, 2021). The model uses four grades of shipbuilding steel: AH36, DH36, AH50, and DH50. The difference between AH and DH grade steels is only the expected temperature at which there would be an impact force, so for the purposes of this research the material properties are the same. Because of this, only two material models were created, one for HS36 (AH36/DH36) steel and one for HS50 (AH50/DH50) steel. The properties input into the cards are shown in Table 3-2.

Table 3-2: Steel Properties

	AH36/DH36	**AH50/DH50**
Mass Density (kg/m^3)	7850	7850
Yield strength (MPa)	355	500
Young's Modulus (GPa)	207	207
Poisson's Ratio	0.3	0.3
Tangent Modulus	N/A	N/A

Yield strength is the point at which the steel ceases to act in an elastic manner, and begins to experience plasticity, or permanent deformation. The Young's modulus is the rate of change of stress versus strain in the elastic region of the stress-strain curve. Poisson's ratio is the proportion at which an object thins laterally when stretches longitudinally. It is considered constant for steel at 0.3 for elastic behaviour. Tangent modulus is the slope of the linear region of a curve. In this case, LS-Dyna ignores the tangent modulus because a load curve is defined in the same card.

Using Appendix 2 from the ABS guidance notes for non-linear finite element analysis, the true flow curves for HS36 and HS51 steels were obtained (ABS, 2021). In consultation with project partners, HS51 steel was deemed to be an acceptable substitution for HS50 steel properties for the purpose of this research since the HS50 flow curves were not available in the document. The data points from these curves were then documented and assigned a *DEFINE_CURVE card in LS PrePost. This card was then called within the

"LCSS" section of the *MAT_024_PIECEWISE_LINEAR_PLASTICITY card to define all parameters of the steel. These flow curves are shown in Figures Figure 3-25 and Figure 3-26.

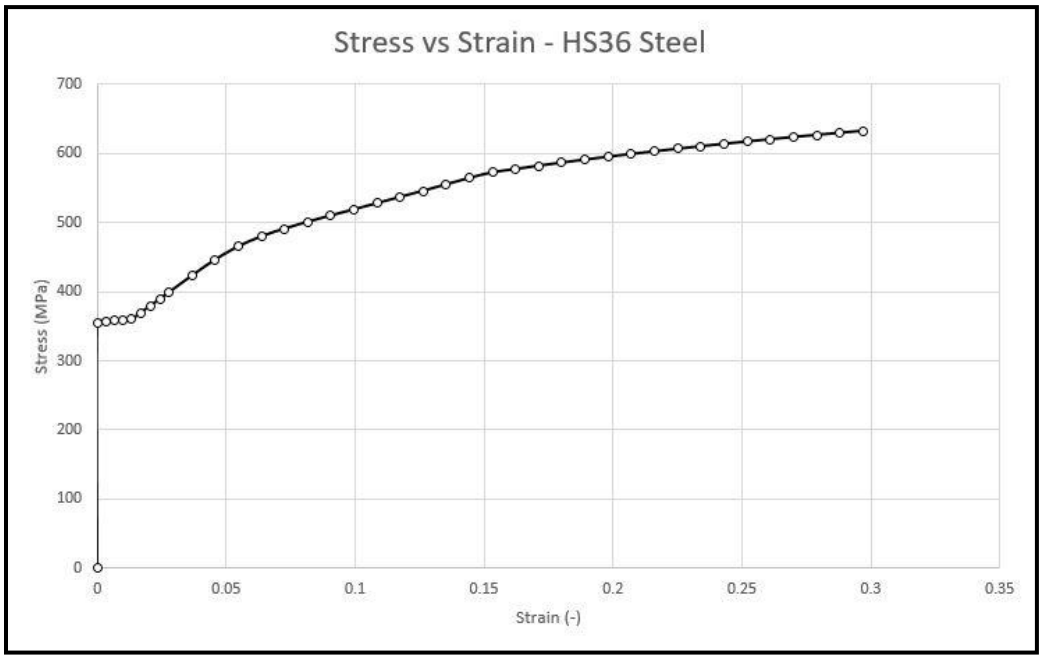

Figure 3-25: Flow Curve - HS36 Steel

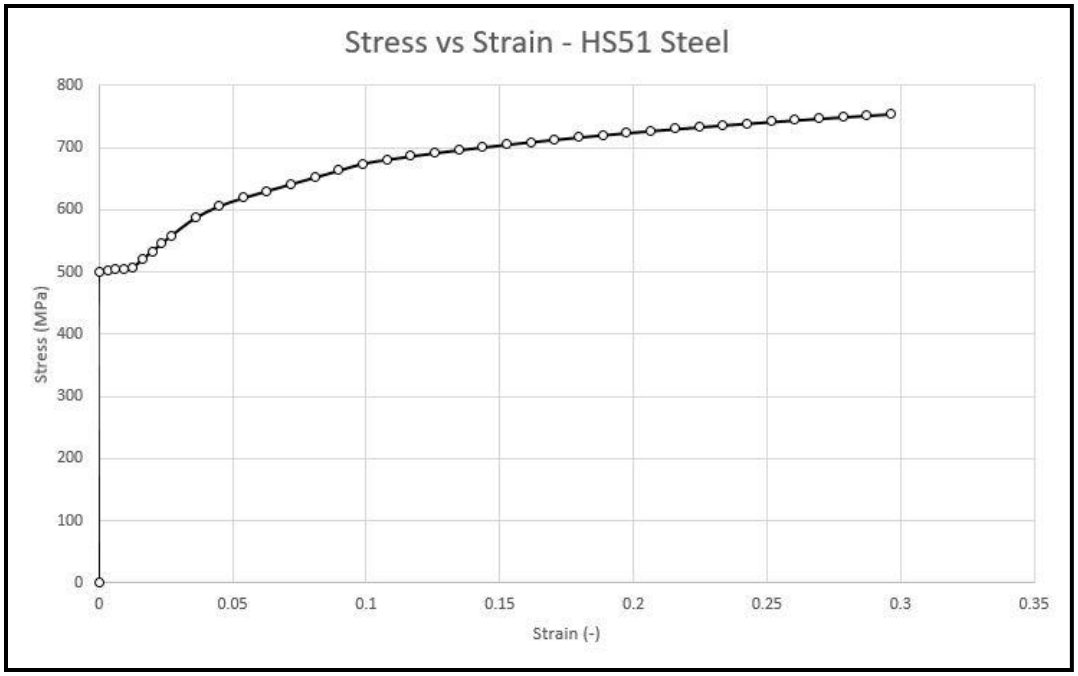

Figure 3-26: Flow Curve - HS51 Steel

The specific values used for these curves can be found in Appendix A Flow Curve Data for HS36 and HS51 Steels.

3.11 Applied Load

The applied load for the analysis was determined from the IACS Polar Rules for design loads. The design load varies depending on factors such as the longitudinal location and vertical section of the ship that is modeled, the principal particulars of the vessel, and the polar class. In the case of this research, the midbody of the Polar Class 2 vessel was analyzed along the ice belt. The IACS Polar Rules give the width and height of the load patch along with the magnitude of the force to be applied. They are determined by using equations 1 and 2 for the force and line load respectively (IACS, 2016).

$$F_{NonBow} = 0.36 * CF_c * DF\ [MN] \quad (1)$$

$$Q_{NonBow} = 0.639 * F_{NonBow}{}^{0.61} * CF_D\ [MN/m] \quad (2)$$

Where:

- CF_C = Crushing failure Class Factor
- DF = Ship displacement factor
    - = $D_{UI}^{0.64}$ if $D_{UI} \leq CF_{DIS}$
    - = $CF_{DIS}^{0.64}$ if $D_{UI} > CF_{DIS}$
- D_{UI} = displacement (not to be taken as less than 10 kilotonnes)
- CF_{DIS} = Displacement Class Factor
- CF_D = Load patch dimensions Class Factor

The "Class Factors" mentioned in the above definitions are based on the IACS Polar Requirements Section I2 and are given in Table 3-3.

Table 3-3: Class Factors (IACS, 2016)

Polar Class	Crushing failure Class Factor (CF_C)	Flexural failure Class Factor (CF_F)	Load patch dimensions Class Factor (CF_D)	Displacement Class Factor (CF_{DIS})	Longitudinal strength Class Factor (CF_L)
PC1	17.69	68.60	2.01	250	7.46
PC2	9.89	46.80	1.75	210	5.46
PC3	6.06	21.17	1.53	180	4.17
PC4	4.50	13.48	1.42	130	3.15
PC5	3.10	9.00	1.31	70	2.50
PC6	2.40	5.49	1.17	40	2.37
PC7	1.80	4.06	1.11	22	1.81

Using the above table, a CF_c of 9.89 was used for the PC2 vessel along with a CF_D of 1.75 and a CF_{DIS} of 210. Since the D_{UI} or displacement of the vessel is 23.50 kilotonnes (and thus less than 210), DF was calculated as $23.5^{0.64}$ which is equal to 7.54.

Using these loads, the dimensions of the load patch was calculated using equations 3 and 4.

$$w_{NonBow} = \frac{F_{NonBow}}{Q_{NonBow}} \ [m] \tag{3}$$

$$b_{NonBow} = \frac{w_{NonBow}}{3.6} \ [m] \tag{4}$$

Where:

- w_{NonBow} = Width of load patch
- b_{NonBow} = height of load patch

A hull area factor was also applied. This hull area factor changes depending on the polar class, region of the load on the ship, and the expected load in that area. There is also a separate set of hull area factors for ships with the "icebreaker" notation. The "icebreaker" table, as shown in Table 3-4, was used for these calculations. From this table, the "PC2" column was used as it matches the class of the vessel, and the "Midbody Icebelt" factor of 0.65 was used as this matches the region of the ship that was modeled. This factor is multiplied by the force. With this calculation completed, the average pressure and design patch dimensions were obtained.

Using the values found above in equations 1 through 4:

$$F_{NonBow} = 0.36 * 9.89 * 7.54 * 0.65 = 17.45\ [MN]$$

$$Q_{NonBow} = 0.639 * 17.45^{\,0.61} * 1.75 = 6.40\ [MN/m]$$

$$w_{NonBow} = \frac{17.45}{6.40} = 2.728\ [m]$$

$$b_{NonBow} = \frac{2.73}{3.6} = 0.758\ [m]$$

The uniform pressure within the patch was then calculated using the following equation.

$$P_{avg} = \frac{F_{NonBow}}{b * w} = \frac{17.45}{0.758 * 2.728} = 8.445\ [MPa]$$

Table 3-4: Hull Area Factors (IACS, 2016)

Hull area		Area	Polar Class						
			PC1	PC2	PC3	PC4	PC5	PC6	PC7
Bow (B)	All	B	1.00	1.00	1.00	1.00	1.00	1.00	1.00
Bow Intermediate (BI)	Icebelt	BI_i	0.90	0.85	0.85	0.85	0.85	1.00	1.00
	Lower	BI_l	0.70	0.65	0.65	0.65	0.65	0.65	0.65
	Bottom	BI_b	0.55	0.50	0.45	0.45	0.45	0.45	0.45
Midbody (M)	Icebelt	M_i	0.70	0.65	0.55	0.55	0.55	0.55	0.55
	Lower	M_l	0.50	0.45	0.40	0.40	0.40	0.40	0.40
	Bottom	M_b	0.30	0.30	0.25	0.25	0.25	0.25	0.25
Stern (S)	Icebelt	S_i	0.95	0.90	0.80	0.80	0.80	0.80	0.80
	Lower	S_l	0.55	0.50	0.45	0.45	0.45	0.45	0.45
	Bottom	S_b	0.35	0.30	0.30	0.30	0.30	0.30	0.30

Based on the above calculations, a pressure of 8.445 MPa was applied over a load patch with a width of 2.728 m and a height of 0.758 m. The load was applied uniformly over the patch at a direction normal to the patch.

This load was applied at the design waterline of the vessel as this is where the vessel is most likely to come into contact with ice. Ice has a density of about 900 kg/m^3. Fresh water has a density of about 1000 kg/m^3 while salt water has a density of about 1025 kg/m^3. Because of this difference in densities, the draft of a piece of ice in salt water would be 900/1025, or about 90%. The design draft of the vessel is 10.5m and the height of the load patch is 0.758m. 10% of the area of this patch should be above the design waterline. 10% of 0.758m is 0.0758 m. Adding this to a design waterline of 10.5 m gives roughly 10.576 m. So, for 90% of the load patch to be below the waterline, the top of the load patch must be located at 10.576 m above baseline. This is displayed in Figure 3-27.

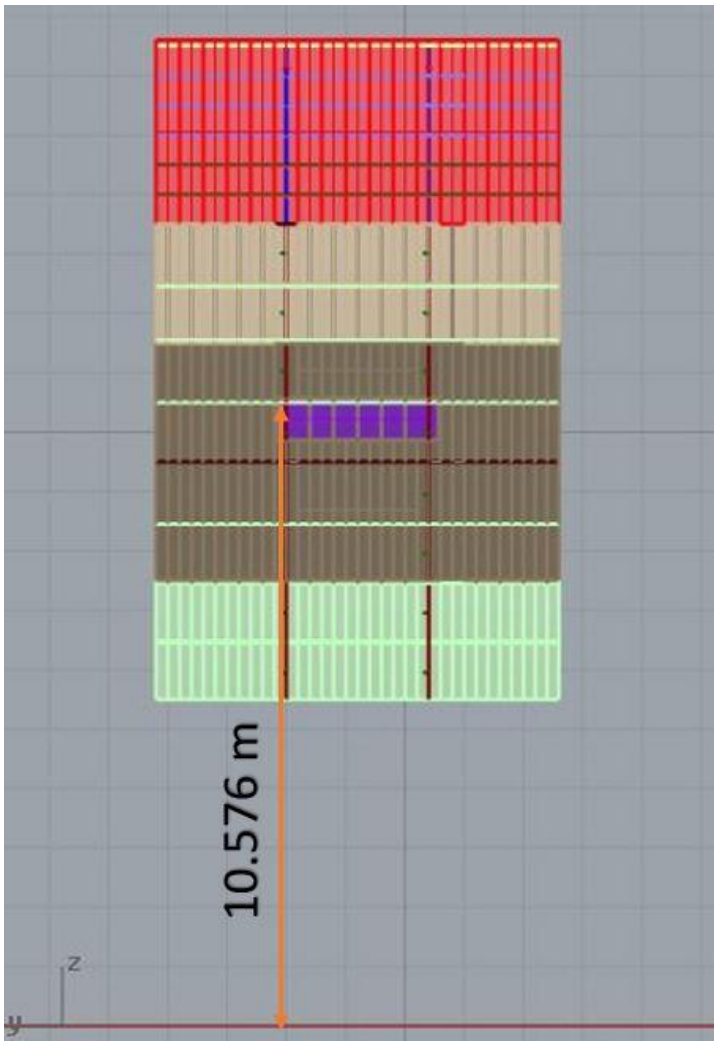

Figure 3-27: Full Model with Load Patch

This pressure patch was applied to various locations during the simulations. It was always centred at the ice strengthened region of the midbody between two central web frames, but the vertical location varied. Along with the design waterline case there were three other vertical load patch locations. The four vertical locations were:

- Load patch edge aligned with the edge of the stringer
- Load patch centred on the stringer

- Load patch centred between two stringers
- Load patch located at the design waterline

With a load patch centred on a stringer, it is possible to study the load case where the frame is expected to experience maximum shear. For this case, the top of the load patch was located 10.86 m above baseline. For the load patch centred between stringers, the load patch was applied directly between two longitudinal stringers where the top of the load patch was 11.36 m above baseline. This case allows for the study of the load case where the structure is expected to experience the highest level of bending and membrane stresses. Finally, a case where the bottom edge of the load patch is aligned with a stringer. The structure in this load case was expected to show a response that was a mix of the previous two load cases. The top of this load patch was located 11.21 m above baseline.

To apply a load, a load curve must also be defined. To do this, the *DEFINE_CURVE card was used. This card defined a pressure time-history curve that tells the *LOAD_SEGMENT_SHELL card the times at which to apply certain portions of the final load. The ordinate and abscissa coordinates (x and y) are treated as time and pressure respectively. This allows the user to change the load over the time of the simulation. In this case, the design load pressure of approximately 8.44 MPa was applied to each node. At time zero there is no load applied. At time equals one second, the full pressure of 8.44 MPa is applied. By defining these two data points, the corresponding load curve will be a linear plot increasing from zero to the full pressure at one second. The load was then ramped back down to zero over the course of 0.5 seconds and subsequently held at 0 for another 0.1

seconds. This ramp down was to allow for the residual behaviour of the structure to be observed. Residual behaviour is the response of the structure after the peak load decreases back down to zero. It represents the permanent response of the structure. The curve card is shown in Figure 3-28.

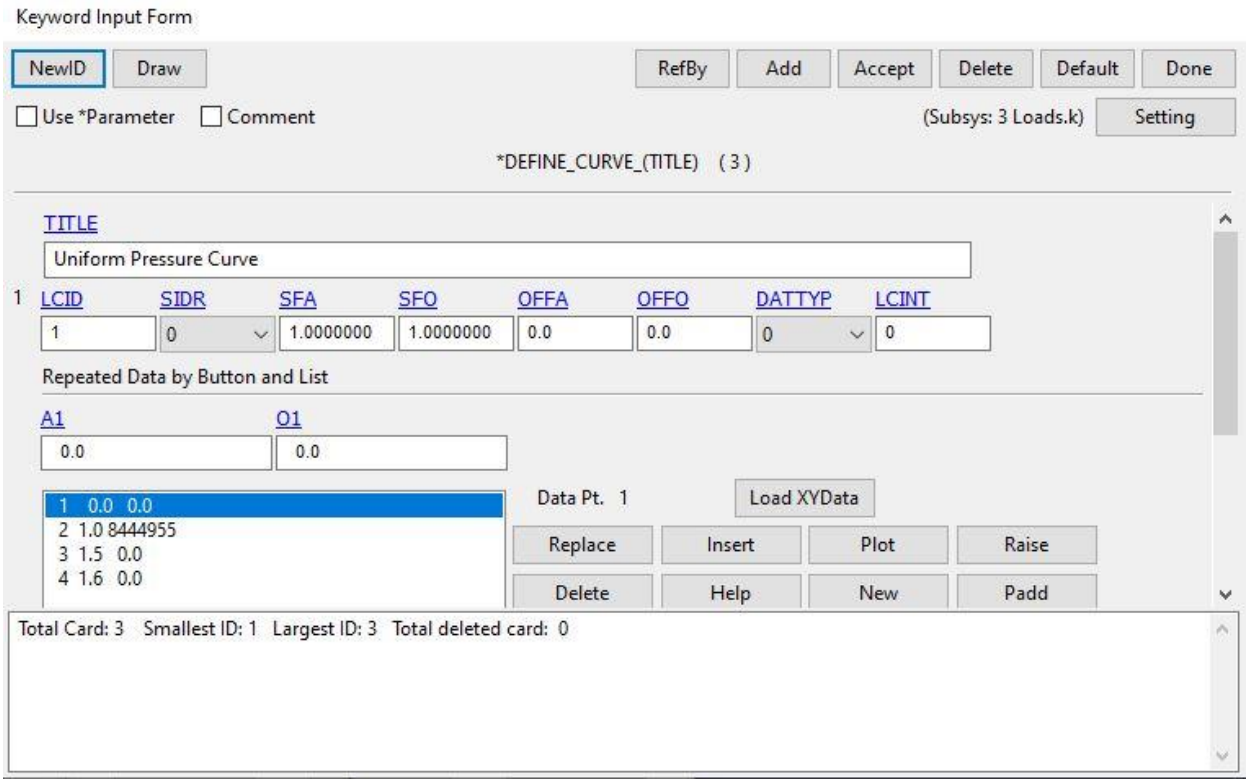

Figure 3-28: Load Curve Card - Residual

The responses for the peak load case were taken at time=1.0 seconds while the residual results were taken from time=1.5 seconds.

To define the elements that experienced the pressure, the *LOAD_SHELL_SET card in LS-Dyna was used. This allows the user to manually define a set of shell elements then select a defined curve to apply to each selected element. A load patch was defined for each

of the four loading conditions described in 3.11. See Figure 3-29 through Figure 3-32 for the four load patch locations.

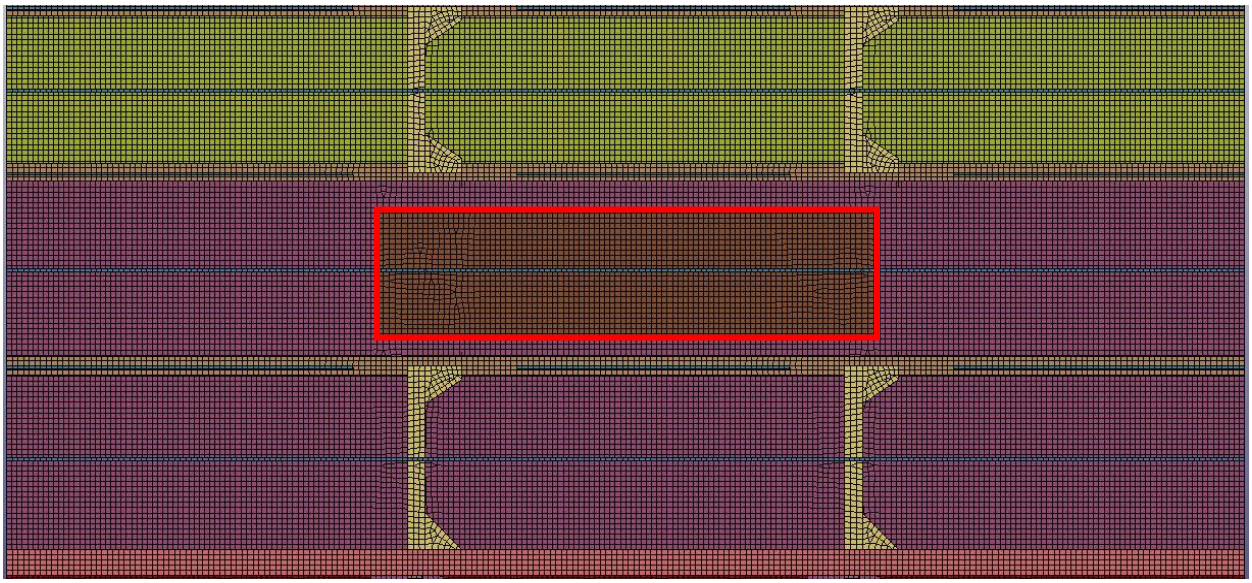

Figure 3-29: Load Location - Centred Between Stringers

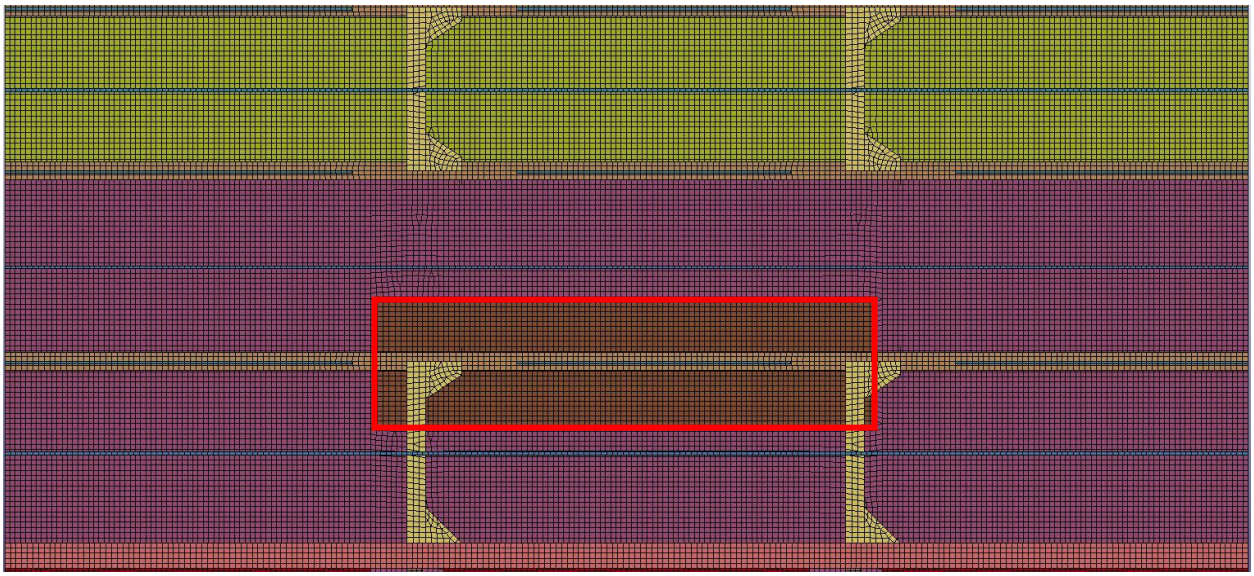

Figure 3-30: Load Location - Centred On Stringer

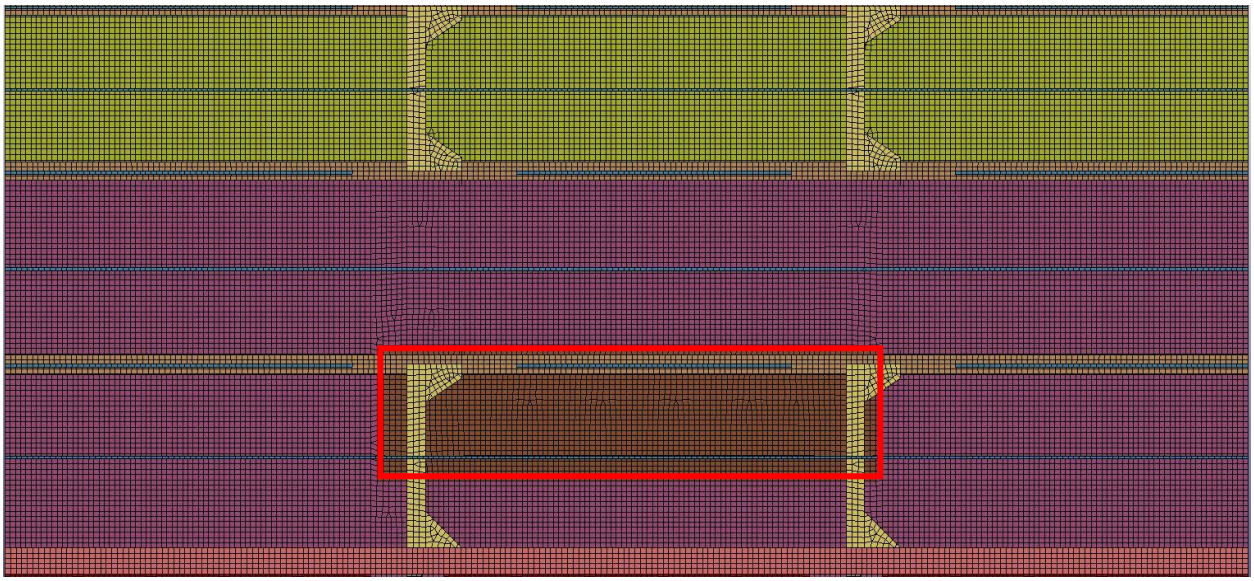

Figure 3-31: Load Location - Design Waterline

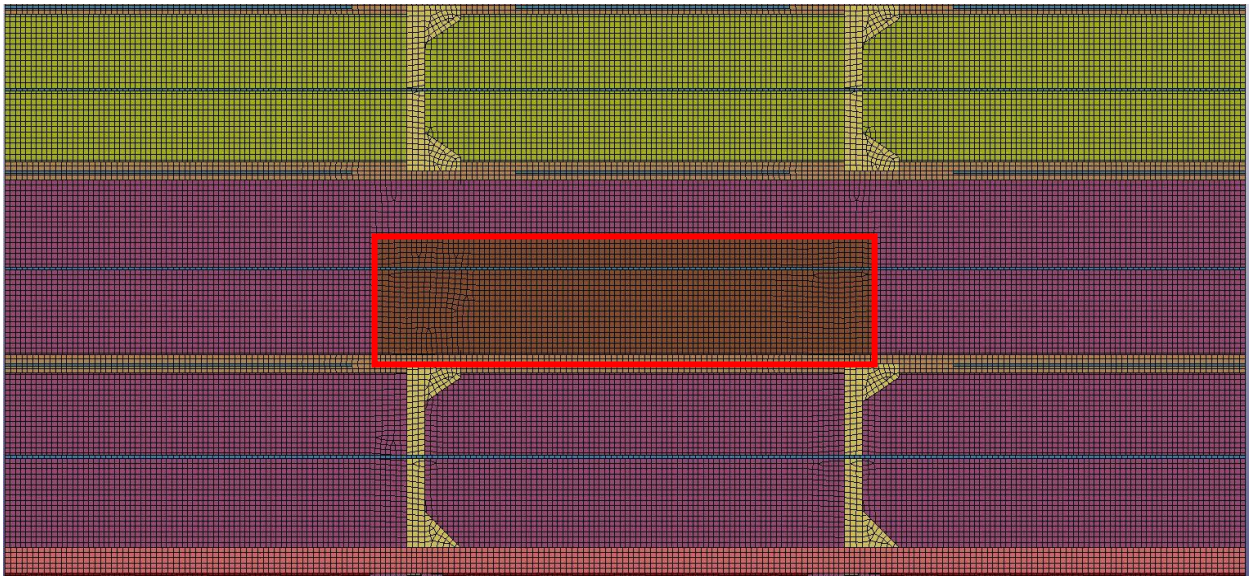

Figure 3-32: Load Location - Edge of Stringer

3.12 Solution Controls

Having proper controls and outputs from an FEA run is a necessary step toward achieving meaningful results. One such step is setting a termination time for the model. Without this,

the simulation would stop after the default “time” set by LS-Dyna which is quite short. To implement this control, the *CONTROL_TERMINATION card was used. This card allows the user to manually input the desired time at which the simulation will terminate. For this project, a termination time of 1.6 seconds was used for each run, while, again, the results for the peak load were taken at time=1.0 seconds and residual results taken at time=1.5 seconds.

Outputs of LS Dyna runs are required to check the necessary results of a simulation such as stress, strain, resultant displacement, etc. For these outputs to be generated, the *DATABASE keywords are used. For this research, the frequency of outputs were defined using the *BINARY_D3PLOT card. As the LS-Dyna database guide (2011) states:

“The output at a given time, called a state, contains a time word, global variables such as total energies and momenta for the whole model and each material (part), node data consisting of displacements, velocities, accelerations, and optionally temperatures, and finally element data that can include stresses and strains at integration points, and element deletion flags.”

By calling D3PLOT information from the database, the user is able to view D3PLOT files for each time step chosen. The time step chosen for the *BINARY_D3PLOT in these simulations was 0.1. This card is shown in Figure 3-33.

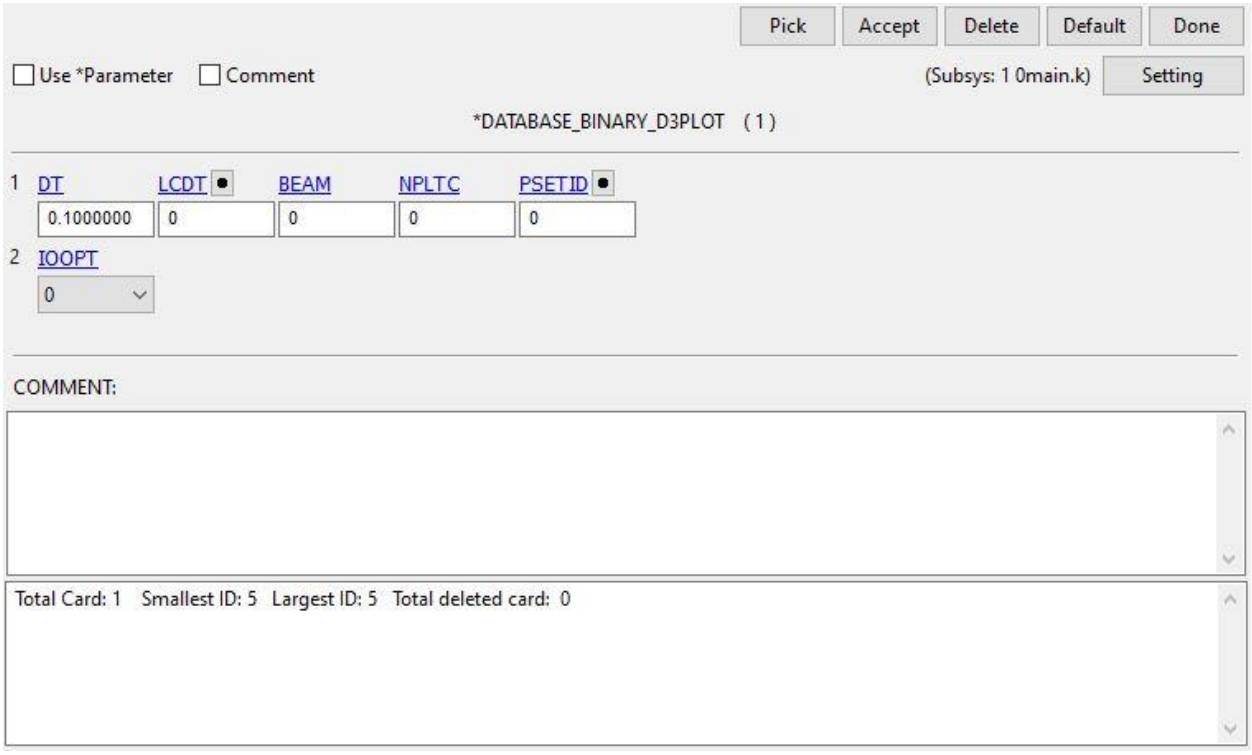

Figure 3-33: *DATABASE_BINARY_D3PLOT CARD

American Standard Code for Information Interchange (ASCII) files in the database section of LS-Dyna are used to produce outputs with a higher resolution. In the *DATABASE_ASCII_option card, the user defines which outputs they want and at which frequency the outputs are generated. ASCII outputs are generated at each step of the simulation. To ensure all ASCII outputs were able to be generated at each step, a resolution of one ASCII output every 0.001 seconds, was chosen. Since the smallest increment size was 0.1 with the auto-stepping simulations never having steps under a size of 0.1, this ensured that an ASCII output was accurately generated at each time step. For each simulation, the following ASCII options were selected:

- BNDOUT to view the forces and energy at the boundary conditions during the simulation
- GLSTAT to view the global statistical properties of the simulation
- MATSUM to view the material properties of the simulation
- SPCFORC to view the reaction forces at the nodes during the simulation

3.13 Failure Criteria

To arrive at meaningful conclusions from the simulations, failure criteria needed to be defined. Without failure criteria for the structure, there is no way to know whether a given connection design is acceptable or not. Failure criteria were developed from various sources. The first failure criterion was based on the ABS Guidelines for Ice Class (ABS, 2005) which states in Section 5.3 that "Permanent deformation of the side shell between longitudinals up to 2% of longitudinal spacing is acceptable." This indicates that any permanent deformation over 2% of the longitudinal spacing is considered inadequate. Permanent deformation means deformation that is still on the structure after the load is removed (i.e. residual deformation). To check for permanent deformations runs are required where the load is ramped down to zero after having already applied the entire load.

The second failure criterion was proposed by Bobeldijk et al (2021). This failure criterion states that the resultant out of plane shell displacement between stiffeners should not exceed 1.5% of the stiffener spacing.

Finally, the third failure criterion was proposed by Pearson et al (2015) who analyzed structural responses of various ice-breaking ships. From these analyses, a simple failure criterion was proposed that no part of the structure may reach an effective plastic strain of 2.5% or higher until the structure is experiencing 150% of the design load. This criterion is simple to observe, however, as Valtonen et al. (2020) mention, effective plastic strain is dependent on mesh size. This means that the same structure under the same load may pass this criterion with one mesh size and fail with another. This failure criterion was not considered to be as important as the resultant displacement criteria for these reasons. However, it was still considered valuable to observe high strain concentrations on the structure.

Chapter 4 Numerical Results

Most of the effort required throughout this project was creating the model of the PC 2 vessel. A large portion of time was spent determining the vertical and inboard extent of the model to achieve a balance between computational efficiency and accuracy of results. The research mainly focused on evaluating different connection designs that may not be typically considered in this region of the vessel to see if they achieve a satisfactory level of structural integrity. A design was considered a failure if one or more of the failure criteria was met for any load location. The structural reactions at the peak load were observed along with the structural reactions of the model after the load was ramped up from zero to the peak load then back down to zero. This condition is referred to as “residual” for all following subsections.

4.1 Fully Welded Collar

The first case to be analyzed was the base case of a fully welded collar around the connection. This is the current design practice and should pass all failure criteria. The welded case was expected to exhibit the strongest structural response across all load locations. This connection design has the most material available to absorb the applied load. Both the peak and residual responses were analyzed as they each give important information about the integrity of the structure.

4.1.1 Peak Load

The centred between stringers load location was the first observed. This was expected to be the load resulting in the most significant structural response. The maximum resultant out of plane shell displacement was observed to be 18.47 mm. This maximum resultant displacement was observed in the vertical centre of the load patch between the central vertical stiffener and the stiffener immediately forward of it. The only notable resultant displacements occurred in the regions between the vertical stiffeners with virtually no displacements occurring outside these areas. The stress was concentrated mainly between vertical stiffeners, at the inner edge of the vertical stiffeners, the flange of the stringers above and below the load patch, near the most forward and aft penetrations in both stringers, and around transitions of the stiffeners and stringers to supporting brackets. The maximum Von Mises stress was located in the centre of the load patch between the central stiffener and the stiffener immediately forward of it. The maximum Von-Mises stress observed on the structure was 505.25 MPa. The effective plastic strain was the final thing to be checked. The maximum effective plastic strain was located on a supporting web frame

stiffener near the aft-most region of the load patch. This was observed to be a strain of 1.85%. This, however, appeared to be an anomalous stress concentration, perhaps due to mesh size. When this stiffener was removed from the results, the maximum effective plastic strain was observed to be 0.8% on the innermost side of the central vertical stiffener.

The next case analyzed was that of the centred on stringer case. The maximum resultant displacement was observed to be 13.01 mm. This displacement was found in the same location as in the centred between stringers case: just above the stringer between the central vertical stiffener and the stiffener immediately forward of it. The most notable resultant displacements occurred in the regions between the vertical stiffeners with some displacement of about 11 mm found in the web of the longitudinal stringer. The maximum out of plane stringer displacement, however, was only 3.94 mm. The stress was concentrated in multiple regions. Yield strength was surpassed in the shell in the region of the load patch, around the fully welded collar on the forward-most and aft-most vertical stiffeners, on the flange of the longitudinal stringer, on the innermost edges of the vertical stiffeners, and at the edges of the connecting brackets for the stiffeners and stringer. A maximum von Mises stress of 506.6 MPa was observed on a bracket connecting the longitudinal stringer to a web frame stiffener on the aft end of the load patch. The stress was centralized on a triangular element. This may indicate an anomalous stress concentration due to element shape and size. Removing this bracket from the results shows that the maximum stress was 503.0 MPa. The effective plastic strain was the final thing to be checked. The maximum effective plastic strain was located on the same connection bracket that bore the maximum stress on the longitudinal member near the aft-most region

of the load patch. This was observed to be a strain of 1.09%. This, however, appeared to be an anomalous stress concentration, perhaps due to mesh size or due to the triangular nature of the shape of the element. When this bracket was removed from the results, the maximum effective plastic strain was observed to be 0.36% around the collar weld on the aft-most vertical stiffener within the width of the load patch.

The case with the load patch applied at the design waterline was next to be analyzed. As expected, the results from these simulations were very similar to the prior run with the load centred on the stringer. The maximum resultant displacement of this simulation was observed to be 12.41 mm. This displacement was found in essentially the same location as the previous two simulations: in line with the load patch located in the gap between the central vertical stiffener and the stiffener immediately forward of it. The most notable resultant displacements occurred in the regions between the vertical stiffeners with some displacement around the central vertical stiffener in the region of the fully welded collar penetration through the stringer. This stringer displaced 9.56 mm, but only 3.57 mm out of plane. The stress was concentrated in the same regions as the centred on stringer case, including a notable concentration at the tip of a connecting bracket of 504.9 MPa. Again, this concentration is likely due to the size of the mesh and shape of the element. Not including this bracket, the maximum stress was observed to be 503.4 MPa. The effective plastic strain results were also similar to the prior case. Most of the strain concentrations were along the vertical stiffeners where they are in line with the load patch. The highest plastic strain was found to be 1.20% at the corner of a supporting web frame stiffener that

intersects with the side shell. Not including this concentration, the highest plastic strain on any main stiffeners, stringers, or side shell was only found to be 0.45%.

The final case to be analyzed for the fully welded collar design was one with the edge of the load patch aligning with the lower longitudinal stringer. The structural response was expected to be similar to that of the centred between stringers case. The maximum resultant displacement was observed to be 17.86 mm. This maximum displacement was found in essentially the same location as the previous two simulations: in line with the load patch located in the gap between the central vertical stiffener and the stiffener immediately forward of it. The most notable resultant displacements occurred in the regions between the vertical stiffeners with some displacement around the central vertical stiffener in the region of the fully welded collar penetration through the stringer. This stringer displaced 10.63 mm, but only 5.05 mm out of plane. The stress profile for this simulation was very similar to the profile of the centred between stringers case. Once again, there was a concentration on the same element mentioned in the previous two simulations. The stress at this location was 505.3 MPa. Not including this anomalous concentration, the maximum von Mises stress observed was 504.7 MPa. The effective plastic strain results were the final thing to be checked. Most of the strain concentrations were along the vertical stiffeners where they are in line with the load patch. The highest plastic strain was found to be 1.52% at the corner of a supporting web frame stiffener that intersects with the side shell with another concentration at the same corner of the bracket as mentioned in the stress discussion. Not including these concentrations, the highest plastic strain on any main stiffeners, stringers, or side shell was only found to be 0.70%.

4.1.2 Residual

Along with the peak load responses, the residual responses were analyzed. The first case to be checked was the centred between stiffeners load patch. The maximum resultant displacement was observed to be 1.48 mm. This displacement was located mainly between the vertical stiffeners in line with the load patch. This maximum displacement was found in essentially the same location as the previous simulations: in line with the load patch located in the gap between the central vertical stiffener and the stiffener immediately forward of it. No displacements other than in way of the outer shell exceeded 1 mm. The next thing to be checked was the residual stress. The maximum residual stress was observed to be 392.9 MPa located on the outer edge of the web of the centre vertical stiffener with other concentrations of less than 300 MPa of stress located along the intersection of the load patch with the vertical stiffeners on the outside of the side shell. The yield strength for these stiffeners is 500 MPa. As for plastic strain, the pattern of the strain itself was nearly identical to that of the peak load simulation. The residual plastic strain was at its highest at the innermost edge of the web of the central vertical stiffener. This strain was observed to be 0.46%.

The centred on stringer case exhibited similar behaviour to the peak load case with some notable exceptions. The highest resultant displacement was observed to be 0.14 mm in way of the load patch between the vertical stiffeners. This level of residual resultant displacement is not significant at all and can be ignored when it comes to significant structural response. The residual von Mises stress pattern of the structure was also observed. The maximum residual von Mises stress was only 138 MPa at the edge of the

welded collar of the aft-most vertical stiffener in way of the load patch. This residual stress value was much lower than the centred between stringers case. The maximum plastic strain observed was 0.17%. This means there was no significant residual plasticity in the structure.

The next case analyzed was the case where the load patch was located at the design waterline. The residual resultant displacement was found to have a maximum value of 0.36 mm in the same location as the peak load simulation: between the central vertical stiffener and the one immediately forward in way of the load patch. The stress profile for the residual case was similar to that of the peak load case with stress being concentrated in many of the same regions of the model. There were, however, some significant stress concentrations at sharp corners within the model. These include the same locations on web frame stiffeners mentioned in the peak load case. There was a concentration of over 500 MPa of stress on the same triangular corner element mentioned earlier and a concentration of 358.6 MPa on the corner of a flatbar web stiffener where it intersects with the load patch. As for the main structure, the highest residual stress observed in the side shell, vertical stiffeners, or longitudinal stringer, was 263.7 MPa located in the region where the load patch intersects the vertical stiffeners. Finally, the plastic strain was checked. Once again, the flatbar web frame stiffener had a concentration on the same corner element of 0.94%. Excluding this concentration, the highest plastic strain was observed to be 0.26% in the same region as the stress profiles. These low values of residual displacement, stress, and plastic strain indicate that there is no significant threat to the structural integrity.

Finally, the load patch aligned with the edge of the longitudinal stringer was analyzed. The maximum resultant displacement was observed to be 1.28 mm in the same location as in the peak load case with the same pattern being observed. The stress profile of the edge case was essentially the same as the profile from the centred between stringers case. Notably, the stress was concentrated on the same corners of web frame stiffeners as discussed in previous sections. Excluding these concentrations, the highest residual von Mises stress observed was 349.5 MPa where the load patch intersects the vertical stiffeners. The plastic strain pattern was once again similar to the other residual load runs, with a peak plastic strain of 0.42% where the load patch intersects the vertical stiffeners.

4.2 Slot Penetration

A slot penetration design was next. This design would save the most in construction costs as there is no welding and no extra steel at all in the penetration region. However, with no welding and no extra supporting steel, this design was expected to exhibit the worst structural performance. Higher stresses, displacements, and strains were expected.

4.2.1 Peak Load

When analyzing the centred between stringers design, the maximum resultant displacement was the first thing to be checked. It was observed to be 23.69 mm between the central vertical stiffener and the stiffener immediately forward of it. There was also out of plane displacement in the stringer web equal to 4.09 mm. The stress profile for this case showed that much of the ice strengthened region yielded when under the design ice load. The peak stress was observed to be 598.3 MPa at the corner of the forward-most penetration where

it intersects with the load patch. Yield strength (500 MPa) was reached at the tip of most penetrations. Finally, the effective plastic strain was checked. The peak plastic strain was observed at the same corner element as the peak stress. This strain was observed to be 3.97%. Other significant regions of plastic strain include at the tips of the forward and aft-most penetrations within the boundaries of the load patch, along the side shell where the load intersects the vertical stiffeners, and the base of the uppermost stringer along the side shell.

The centred on stringer case was next. The peak resultant displacement observed in this simulation was 16.93 mm in the same location relative to the load patch as all other simulations. There was also displacement observed in the stringer of 14.89 mm, with 4.88 mm out of plane displacement of the web. The stress pattern of this simulation was then checked. The peak stress was observed to be 608.4 MPa in the stringer web just off of the tip of the forward-most penetration. The stress was generally concentrated at the tip and base of most penetrations and all along the load patch. Yield strength was reached in the web of the stringer around four of the five penetrations, along the flange, in various lower grade steel connecting brackets, where both the lower and upper stringer intersect with the side shell, and along the central parts of the vertical stiffeners. The plastic strain was also analyzed. The stringer web near the forward and aft-most penetrations experienced the highest levels of plastic strain with a peak strain of 4.59% near the forward-most penetration. The main strain concentrations were at the tip and base of these penetrations.

The design waterline case was next to be examined. The resultant displacement was checked first and a maximum value of 14.75 mm was observed in the same relative region

as prior simulations, There was also some slight displacement in the stringer with 12.06 mm of displacement with 4.57 mm of out of plane web displacement. Next, the stress profile was checked. The stress profile of this case was very similar to the centred on stringer case. The peak stress was slightly lower at 563.9 MPa but this maximum stress was located in the exact same region: near the tip of the forward-most penetration along the load patch. Yield was observed in many of the same regions as the centred on stringer case, but with lower average stresses in the web and flange of the stringer and higher average stress in the vertical stiffeners and lower connecting brackets between the vertical stiffeners and the deck. The plastic strain pattern was checked as well. The stringer web near the forward and aft-most penetrations experienced the highest levels of plastic strain with a peak strain of 2.849% near the forward-most penetration. This is significantly lower (just over half) than the centred on stringer case. While this strain value should be observed with some degree of skepticism due to the face that a change in mesh size can affect strain, the fact that the strain observed here is relatively much higher than other cases suggests that it is significant. The main strain concentrations where yield strength was exceeded were at the tip and base of these penetrations, along with some minor concentrations along the vertical stiffeners where they intersect the load patch.

Finally, the load case on the edge of the stringer was analyzed. First, the resultant displacement was observed to have a maximum value of 22.95 mm in the same relative region to all other simulations. A maximum displacement in either stringer was observed to be 14.46 mm with a maximum out of plane web displacement of 4.72 mm. The stress profile for this run was a lot like the centred between stringers run. A peak stress of 624

MPa was observed which was the highest of all slot penetration cases. The areas of yield strength concentrated near the forward and aft penetrations, along the stringer web and flange, along the intersection of the stringers with the side shell, and along the brackets connecting the vertical stiffeners to the deck. Finally, the plastic strain pattern was observed to also be similar to the centred between stringers case. The peak plastic strain was observed to be 4.78% at the base of the forward-most penetration. The strain was concentrated near the base and tip of the forward and aft-most penetrations with some lighter concentrations being observed along the intersection of the vertical stiffeners and the load patch.

4.2.2 Residual

The centred between stringers case was the first to be examined. The maximum residual resultant displacement was observed to be 3.08 mm in the same region as all prior simulations. As was the case with the peak load, this residual displacement is significantly higher than the fully welded collar case. There was also a maximum residual stringer displacement of 1.31 mm. The general residual stress profile was similar to that of the peak load case. The peak residual stress was 565.9 MPa at the base of the forward-most penetration with other significant concentrations being found near the tips of the penetrations, along the load patch where it intersects the vertical stiffeners, and the base of the stringers where they intersect the side shell. The residual plastic strain was then checked. A peak strain value of 2.94% was observed at the base of the forward-most penetration with other concentrations of strain being where the vertical stiffeners intersect the load patch, and where the stringers intersect the side shell.

The centred on stringer case was next to be examined. The maximum residual resultant displacement was 2.23 mm in the same region as the maximum displacement from other runs. The residual displacement pattern was slightly different from other runs with most of the displacement coming around the web of the stringer near the forward and aft penetrations as well as the inner edge of the forward and aft vertical stiffeners. The highest concentrations of residual stress were around the base and tip of the forward and aft-most penetrations with a peak residual von Mises stress of 594.7 MPa located in the stringer web just off the tip of the forward-most penetration. There were additional stress concentrations where the stringers connect with the side shell and where the vertical stiffeners intersect the load patch. Finally, the plastic strain had a peak residual value of 3.95% in the same element as the maximum stress. Similar to the stress profile, the main regions of plasticity were around the base and tip of the forward and aft-most penetrations on the lower stringer.

Next was the design waterline load case. The maximum residual resultant displacement was only 1.10 mm in the same location as all other runs. The stringer had a maximum residual displacement of 1.03 mm. The stress profile was next to be analyzed. As with the peak load case, the residual stress was mainly concentrated at the base and near the tip of the forward and aft-most penetrations on the lower stringer, plus along the base of the stringer where it intersects the side shell. The highest residual stress was observed to be 532.8 MPa located at the base of the forward-most penetration. The highest residual plastic strain was also found near this penetration, but just off the tip. This strain was 2.07%. The strain was mainly concentrated around the forward and aft-most penetrations.

The final load patch location was the case with the edge of the patch aligned with the edge of the lower stringer. The maximum residual resultant displacement for this was 3.01 mm located in the same relative area as all other simulations. The maximum residual displacement in the stringer was 1.87 mm with a negligible amount of displacement out of plane. The stress profile was observed to be similar to the peak load case and the centred between stringers case for the residual case. Most of the stress was concentrated around the forward and aft-most penetrations on both stringers, along with some residual stress along the region where the vertical stiffeners intersect with the side shell. The maximum stress was observed to be 594.4 MPa at the base of the forward-most penetration on the lower stringer. Finally, the residual effective plastic strain was checked. The maximum plastic strain was observed in the same element as the maximum stress with a maximum value of 3.94%. Strain concentrations were observed in the same region as the residual centred between stringers case: where the vertical stiffeners intersect the load patch, and where the stringers intersect the side shell.

4.3 Penetration Welded on One Side

The welded on one side penetration design was next to be analyzed. This design was expected to perform slightly better than the slot penetration case due to the extra structural reinforcement provided by the weld, however it was not expected to have similar strength to the fully welded collar.

4.3.1 Peak Load

For the centred between stringers load case, the maximum resultant displacement was found to be 21.90 mm in the same region as all other runs. The maximum resultant displacement observed in the stringer was 12.09 mm with a maximum out of plane web displacement of 5.84 mm. The stress profile was found to be similar to that of the slot penetration case for the same load location. The peak von Mises stress was 584.0 MPa. This peak stress was found to be located in the stringer web just off the tip of the penetration on the forward-most penetration of the lower stringer. Yield strength was reached around all but one penetration on the webs of both stringers, along the flange of both stringers, between all vertical stiffeners on the load patch, and along both edges of the vertical stiffeners. The peak effective plastic strain was found to be 3.42% in the same location as the peak stress. Other regions of high strain include around the forward-most penetration on the upper stringer, and along the vertical stiffeners where they intersect the side shell.

The centred on stringer case was the next one to be analyzed. The maximum resultant displacement of this run was 15.97 mm. The stringer displaced 13.93 mm with 4.56 mm out of plane stringer web displacement. The stress profile was once again similar to the same load location as the slot penetration with a maximum von Mises stress observed to be 601.2 MPa just off the tip of the forward-most penetration on the web of the lower stringer. The stress was generally concentrated at the tip and base of most penetrations and all along the load patch. Yield strength was reached in the web of the stringer around four of the five penetrations, along the flange, in various lower grade steel connecting brackets, where both the lower and upper stringer intersect with the side shell, and along the central

parts of the vertical stiffeners. The plastic strain was also analyzed. The stringer web near the forward and aft-most penetrations experienced the highest levels of plastic strain with a peak strain of 4.23% near the forward-most penetration. The main strain concentrations were at the tip and base of these same penetrations.

Next was the design waterline case. The resultant displacement was checked first and a maximum value of 14.20 mm was observed in the same relative region as prior simulations. There was also some slight displacement in the stringer with 11.50 mm of displacement with 4.35 mm of out of plane web displacement. Next, the stress profile was checked. The stress profile of this case was very similar to the centred on stringer case and the same load location in the slot penetration run. The peak stress was slightly lower than the centred on stringer case at 568.6 MPa but this maximum stress was located in the exact same region: at the tip and base of most penetrations and all along the load patch. Yield was observed in many of the same regions as the centred on stringer case, but with lower average stresses in the web and flange of the stringer and higher average stress in the vertical stiffeners and lower connecting brackets between the vertical stiffeners and the deck. The plastic strain pattern was checked as well. The stringer web near the forward-most penetration experienced the highest level of plastic strain with a peak strain of 2.98% near the tip of the forward-most penetration. The main strain concentrations where yield strength was exceeded were at the tips of the forward and aft-most penetrations along the load patch.

The final welded on one side case to be analyzed was the load case on the edge of the stringer. First, the resultant displacement was observed to have a maximum value of 21.45 mm in the same relative region to all other simulations. A maximum displacement in either

stringer was observed to be 13.33 mm with a maximum out of plane web displacement of 4.35 mm. The stress profile for this run was a lot like the centred between stringers run. A peak stress of 604.2 MPa was observed which was the highest of all slot penetration runs. The areas of yield strength concentrated near the forward and aft penetrations on the stringer web, along the stringer flange, along the intersection of the stringers with the side shell, and along the brackets connecting the vertical stiffeners to the deck. Finally, the plastic strain pattern was observed to also be similar to the centred between stringers case. The peak plastic strain was observed to be 4.14% in the stringer web near the tip of the forward-most penetration. The strain was concentrated near the base and tip of the forward and aft-most penetrations with some lighter concentrations being observed along the intersection of the vertical stiffeners and the load patch.

4.3.2 Residual

The centred between stringers case was the first to be examined. The maximum residual resultant displacement was observed to be 2.58 mm in the same region as all prior simulations. As was the case with the peak load, this residual displacement is significantly higher than the fully welded collar case. There was also a maximum residual stringer displacement of 1.25 mm. The general residual stress profile was similar to that of the peak load case. The peak residual stress was 557.8 MPa at the tip of the forward-most penetration on the upper stringer with other significant concentrations being found near the tips and bases of the forward-most and aft-most penetrations, along the load patch where it intersects the vertical stiffeners, and the base of the stringers where they intersect the side shell. Notably, this run was the only one to see yield strength occur near the tip and base

of a penetration that is not the forward-most or aft-most within the load patch region. On the upper stringer, yield was observed at the tip and base of the penetration that is located one spot forward of the central penetration. The residual plastic strain was then checked. A peak strain value of 2.71% was observed at the tip of the forward-most penetration on the upper stringer with another significant concentration just off the tip of the forward-most penetration on the lower stringer. Other concentrations of strain occurred where the vertical stiffeners intersect the load patch, and where the stringers intersect the side shell.

The centred on stringer case was next to be examined. The maximum residual resultant displacement for this was 1.66 mm located in a slightly different region than most other runs. The maximum residual resultant displacement was found to be on the stringer just off the tip of the forward-most penetration with the resultant displacement being concentrated all around this penetration along the stringer, vertical stiffener, and load patch. Next, the residual von Mises stresses were checked. The maximum residual von Mises stress was observed to be 593.2 MPa and was located just off the tip of the forward-most penetration. Other significant stress concentrations were found near the tip and base of the forward and aft-most penetrations, along a bracket connecting the main stringer to a web frame stiffener, and along the base of the stringer where it intersects the load patch. Finally, the residual effective plastic strain was analyzed. The only significant strains were observed at the tip and base of the forward and aft-most penetrations with a maximum strain value of 3.88% being found in the same element as the maximum residual von Mises stress.

Next was the design waterline load case. The maximum residual resultant displacement was 0.95 mm in a slightly different location than the majority of other runs, and a region

somewhat similar to the centred on stringer case. The residual resultant displacement was concentrated on the load patch just aft of the forward-most penetration below the stringer. The stringer itself had a maximum residual displacement of 0.90 mm. The stress profile was next to be analyzed. The residual stress was mainly concentrated at the base and near the tip of the forward-most penetration, along the vertical stiffeners where they intersect the load patch, along a supporting bracket connecting the main stringer to a web frame stiffener, plus along the base of the stringer where it intersects the side shell. The highest residual stress was observed to be 539.7 MPa located just off the tip of the forward-most penetration. The highest residual plastic strain was also found just off the tip of the forward-most penetration. This strain was 2.34%. The strain was mainly concentrated around the tip of the forward and aft-most penetrations.

The final load patch location was the case with the edge of the patch aligned with the edge of the lower stringer. The maximum residual resultant displacement was 2.41 mm in the same region as the maximum displacement from other runs. The highest concentrations of residual von Mises stresses were around the base and tip of the forward and aft-most penetrations on the lower stringer, and the forward-most penetration on the upper stringer with a peak residual von Mises stress of 578.1 MPa located in the stringer web just off the tip of the forward-most penetration on the lower stringer. There were additional stress concentrations where the stringers connect with the side shell and where the vertical stiffeners intersect the load patch with yield strength being reached along the base of the lower stringer. Finally, the plastic strain had a peak residual value of 3.31% in the same element as the maximum stress. Similar to the stress profile, the main regions of plasticity

were around the tips of the forward and aft-most penetrations on the lower stringer and the forward-most penetration on the upper stringer.

4.4 Penetration Welded on One Side with Tab

The final penetration design used was the welded on one side with tab case. Based on experience, this case was expected to exhibit the strongest structural response other than the fully welded collar case.

4.4.1 Peak Load

First, the centred between stringer case was analyzed. The maximum resultant displacement was the first response to be looked at. The peak resultant displacement was observed to be 18.88 mm in the same location as all other runs. There was some minor stringer displacement with a peak value of 10.69 mm with 5.56 mm out of plane web displacement. The stress profile was found to be similar to that of the fully welded collar case for the same load location. The peak von Mises stress was 506.1 MPa. This peak stress was found to be located on the supporting tab on the forward-most penetration of the lower stringer. Yield strength was reached on the tabs of the forward penetrations on both the lower and upper stringer, around the edges of the forward and aft penetrations of both stringers, along the flange of both stringers, and along the inner edge of the vertical stiffeners. The peak effective plastic strain was found to be 1.89% at the corner of a supporting web frame stiffener in way of the load patch. Other than this concentration on the stiffener, the highest plastic strain occurred on the forward-most tab on the lower stringer with a strain of 0.97%.

The centred on stringer case was next. The maximum resultant displacement was the first response to be checked. The peak resultant displacement was observed to be 13.54 mm in the same location as all other runs. There was some stringer displacement with a peak value of 11.55 mm with 3.95 mm out of plane web displacement. The stress profile was found to be similar to that of the fully welded collar case for the same load location. The peak von Mises stress was 510.2 MPa. This peak stress was found to be located near the tip of the penetration on the aft-most part of the lower stringer. Yield strength was reached on the tabs of the forward and aft penetrations on the lower stringer, in the stringer web around the edges of the forward and aft penetrations, along the stringer flange, and along the vertical stiffeners where they intersect the load patch and on the inner edge. The peak effective plastic strain was found to be 1.84% at the tip of the aft-most penetration. However, this element is triangular in shape and smaller than surrounding elements. This is likely resulting in a higher plastic strain value than is truly there. Other than this concentration, the highest plastic strain occurred on the forward-most tab on the stringer with a strain of roughly 1.6%.

For the design waterline case, the maximum resultant displacement was observed to be 12.69 mm in the same relative location as all other runs. There was also some displacement in the stringer with 9.85 mm of displacement with 3.61 mm of out of plane web displacement. Next, the stress profile was checked. The stress profile of this case was very similar to the centred on stringer case and the same load location in the slot penetration run. The peak stress was slightly lower than the centred on stringer case at 506.0 MPa but this maximum stress was located in the exact same region: near the tip of the penetration

on the aft-most part of the lower stringer. Yield was observed in many of the same regions as the centred on stringer case, but with lower average stresses in the web and flange of the stringer and higher average stress in the vertical stiffeners and lower connecting brackets between the vertical stiffeners and the deck. The plastic strain pattern was checked as well. The peak strain was observed to be on a supporting web frame stiffener made of a lighter steel. This strain value was 1.20%. Other than this stiffener, strains of about 1% were found in the forward-most tab and also in the same location as the peak stress just off the tip of the aft-most penetration.

Finally, for the case where the load patch is aligned with the edge of the lower stringer, the maximum resultant displacement was observed to be 18.29 mm in the same relative location as all other runs. The stringer had a maximum displacement of 11.01 mm with 5.42 mm out of plane web displacement. The stress profile for this case was similar to that of the fully welded collar case and was similar to the centred between stringers case. The maximum von Mises stress was 508.5 MPa located on the tab of the forward-most penetration of the lower stringer. Yield strength was reached on the tabs of the forward penetrations on both the lower and upper stringer, around the edges of the forward and aft penetrations of both stringers, along the flange of both stringers, and along the inner edge of the vertical stiffeners. The peak effective plastic strain was found to be 1.57% at the corner of a supporting web frame stiffener in way of the load patch. Other than this concentration on the stiffener, the highest plastic strain occurred on the forward-most tab on the lower stringer with a strain of 1.45%.

4.4.2 Residual

The centred between stringers case was the first to be examined. The maximum residual resultant displacement was observed to be 1.63 mm in the same region as all prior simulations. There was also a maximum residual stringer displacement of 0.41 mm. The general residual stress profile was similar to that of the peak load case. The peak residual stress was 444.2 MPa on a triangular element near the tip of the aft-most penetration on the upper stringer with other significant concentrations being found near the tips of the penetrations, along the load patch where it intersects the vertical stiffeners, and at the corners of a connecting bracket and web frame stiffener made of lighter steel. The residual plastic strain was then checked. A peak residual strain value of 1.60% was observed at the corner of a weaker supporting web frame stiffener with other concentrations of strain being where the vertical stiffeners intersect the load patch, and on the forward-most tab on both stringers.

The centred on stringer case was next to be examined. The maximum residual resultant displacement was 0.39 mm in a different region than all other simulations. The maximum residual resultant displacement occurred in the side shell between the forward-most vertical stiffener and the stiffener immediately aft of it. The residual displacement pattern was slightly different from other runs with most of the displacement coming around the forward-most vertical stiffener web, the stringer in way of the penetration for this stiffener, and in the side shell just aft of this stiffener. The highest concentrations of residual stress were around the base and tip of the forward and aft-most penetrations, on the forward-most tab, and on the corners of brackets that connect the stinger to a web stiffener. The peak

residual von Mises stress of 506.0 MPa was located at the corner of the aforementioned connecting bracket. Other than this concentration of the bracket, the highest residual von Mises stress was observed to be 373.5 MPa on a triangular element at the tip of the aft-most penetration. Finally, the plastic strain had a peak residual value of 1.05% in a triangular element off the tip of the aft-most penetration. Similar to the stress profile, the main regions of plasticity were around the base and tip of the forward and aft-most penetrations on the lower stringer and along the forward-most tab.

Next was the design waterline load case. The maximum residual resultant displacement was only 0.42 mm in the same location as most other runs. The stringer had a maximum residual displacement of 0.18 mm. The residual von Mises stress profile was next to be analyzed. As with the peak load case, the residual stress was mainly concentrated at the base and near the tip of the forward and aft-most penetrations on the lower stringer, along the vertical stiffeners where they intersect the load patch, and on brackets connecting the stringer to a web frame stiffener. The highest residual stress was observed to be 502.1 MPa located at the corner of this same connecting bracket. Other than this bracket and another concentration on a web frame stiffener, the highest residual von Mises stress was found to be 296.5 MPa near the tip of the aft-most penetration. The highest residual plastic strain was found to be on a web frame flatbar stiffener where it intersects the load patch. This strain was 0.93%. The strain was mainly concentrated around the forward and aft-most penetrations, on the supporting tabs, and along the vertical stiffeners where they intersect the load patch.

The final load patch location was the case with the edge of the patch aligned with the edge of the lower stringer. The maximum residual resultant displacement for this was 1.37 mm located in the same relative area as most other simulations. The maximum residual displacement in the stringer was 0.40 mm with a negligible amount of displacement out of plane. The stress profile was observed to be similar to the peak load case and the centred between stringers case for the residual case. Most of the stress was concentrated around the forward and aft-most penetrations on both stringers, on the tab of the forward penetration on the lower stringer, along a connecting bracket between the stringer and a web frame stiffener, on a separate web frame flatbar stiffener where it intersects the load patch, along with some residual stress along the region where the vertical stiffeners intersect with the side shell. The maximum residual von Mises stress was observed to be 504.6 MPa on the connecting bracket mentioned earlier. Other than the concentration on this bracket and another web frame stiffener, the maximum von Mises stress was 342.7 MPa on the web of the centre vertical stiffener. Finally, the residual effective plastic strain was checked. The maximum plastic strain was observed on the corner of a flatbar stiffener on the web frame where it intersects the load patch. This strain was 1.22%. Strain concentrations were observed in the same region as the residual centred between stringers case: where the vertical stiffeners intersect the load patch, around the tips and bases of the forward and aft-most penetrations, and on the forward-most tab on the lower stringer.

4.5 Design Comparisons

As noted in some of the results presented earlier in Chapter 4, some von Mises stress and effective plastic strain concentrations were located on weaker AH36 steel components such

as brackets or small stiffeners. An example of some maximum stress and strain locations are shown in Figure 4-1 through Figure 4-3. These show maximum stress and strain locations for the design waterline load location including the triangular AH36 bracket mentioned, the supporting web frame stiffener, and the location on the stringer web where the highest stress concentrations were observed.

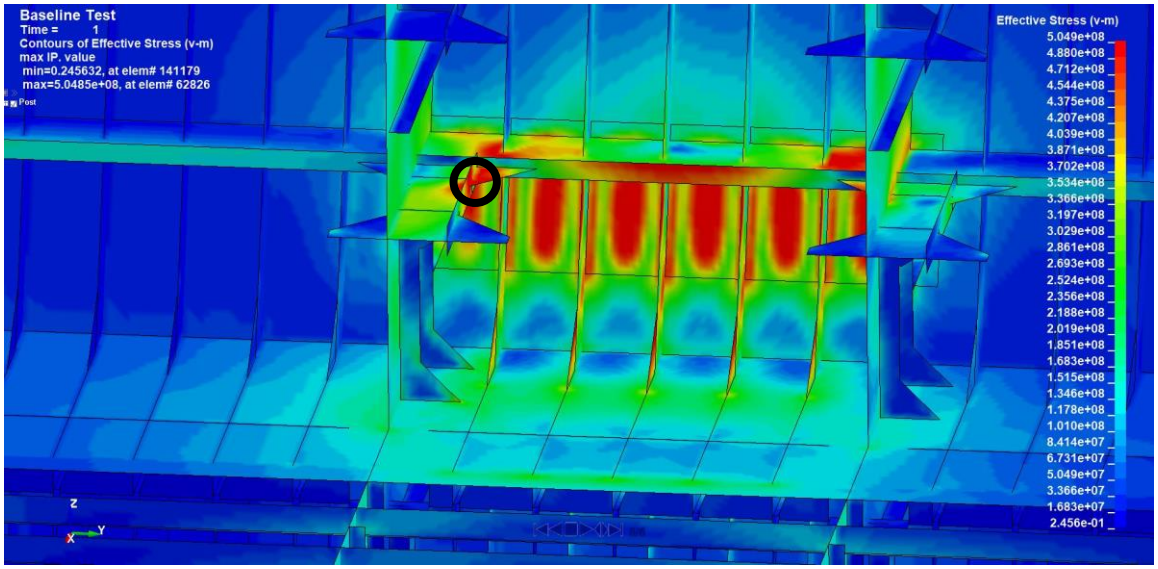

Figure 4-1: Maximum Stress Location - Fully Welded Collar - Design Waterline Load Location

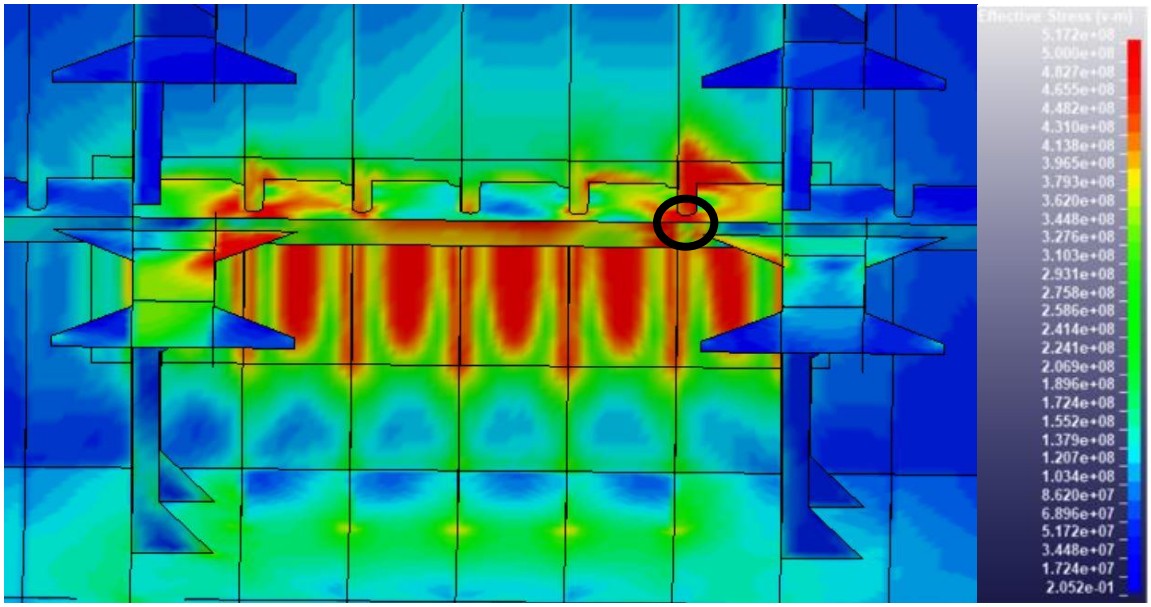

Figure 4-2: Maximum Stress Location - Penetration Welded on One Side - Design Waterline Load Location

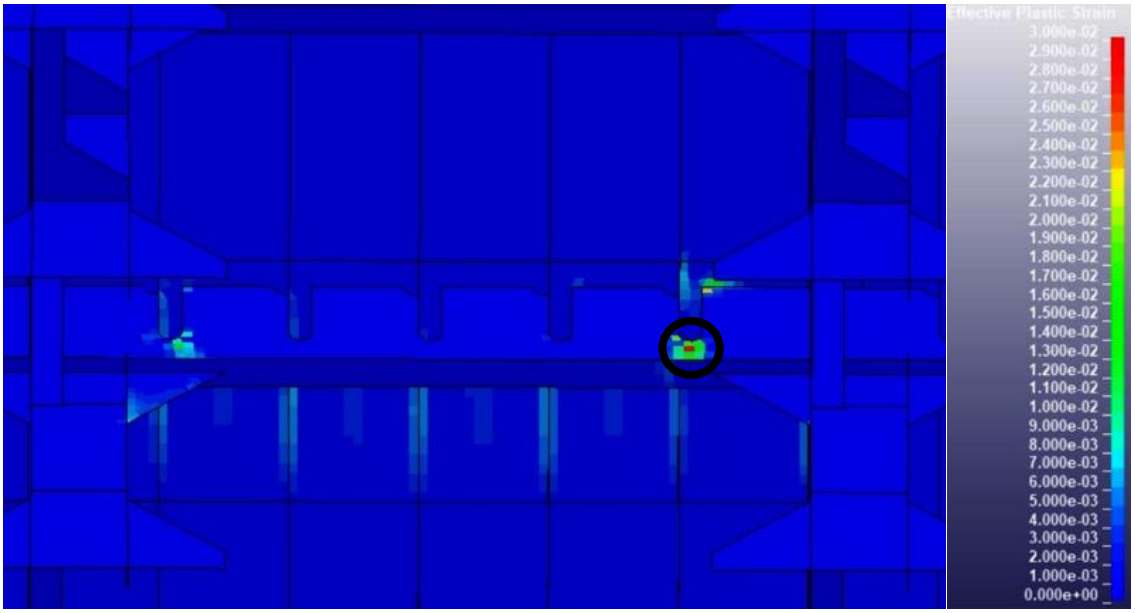

Figure 4-3: Maximum Effective Plastic Strain Location - Penetration Welded on One Side - Design Waterline Load Location

It should be noted that the concentrations observed on these specific AH36 steel structural members may indicate that these steels are not appropriate for this vessel in these specific locations. They indicate that the ice load is not being distributed among the ice reinforced structure as efficiently as desired. This is not studied further in this thesis, however it may be worth studying in the future.

The slot penetration design gave the worst structural performance across all failure criteria for all but one load location. It experienced the largest resultant displacement of all simulations with an out-of-plane shell displacement of 23.69 mm during the centred on stringer load location run. It also experienced the highest plastic strain of all simulations with 4.78% during the edge load location run. The slot penetration failed the plastic strain requirement for all four load locations.

The penetration design with a full weld on one side was expected to perform better than the slot penetration design as it has the same penetration dimensions with an added level of stiffness coming from the weld. In general, this hypothesis held true with only one exception. The resultant displacements were lower than those for the slot penetration for every run, and the plastic strains were lower for all but one run. The design waterline load location for the welded one side case experienced a higher effective plastic strain than the same load location for the slot penetration. The welded one side case failed the plastic strain criteria for the centred between stiffener and edge load locations (the same as the slot penetration case).

The design with a penetration welded on one side with a supporting lug or tab was expected to exhibit the strongest structural response of the three alternative designs. This proved true through the simulations. Throughout all load locations, the welded one side with tab design performed the best of the three, compared to the fully welded collar baseline case. It had the lowest resultant displacements and effective plastic strains across all load locations. The welded one side with tab design performed very similarly to the fully welded collar case. While being the strongest of all alternate designs, this design also passed all failure criteria. The effective plastic strain never reached 2.5% in any run, nor did the resultant out of plane shell displacement ever cross the 2% of the longitudinal spacing or 1.5% of the stiffener spacing.

A matrix of all resultant out of plane shell displacements, displacements as a percentage of longitudinal spacing, displacements as a percentage of stiffener spacing, and effective plastic strains are shown in Table 4-1 through Table 4-9. A red highlight in a cell indicates that the value in that cell failed its respective failure criterion. Please also note that the penetration designs and load locations are abbreviated for simplicity. Fully welded collar (FUSED), penetration welded on one side with tab (TAB), penetration welded on one side (W1S), slot penetration (SLOT), centred between stringers (CBS), centred on stringer (COS), load located on the edge of the lower stringer (EDGE), and design waterline load location (DWL) are all abbreviations found in Table **4-1** to Table **4-9**. From these tables, it was observed that there were strong similarities between the welded one side and slot penetration designs, and the tab and fully welded collar designs across all simulations. There were also similar structural responses for the edge of stringer and centred between

stringer cases, along with the pair of the design waterline and centred on stringer case. A Load-Displacement plot for all CBS cases is provided in Figure 4-4: Force vs Resultant Displacement - All Penetration Designs - Load Centred Between Stringers showing the response of each penetration design to the load.

Table **4-1**: Maximum Design Load von Mises Stress

Maximum Von-Mises Stress (MPa)				
	CBS	COS	EDGE	DWL
FUSED	505.3	506.6	505.3	504.9
TAB	506.1	510.2	508.5	506.0
W1S	584.0	601.2	604.2	568.6
SLOT	598.3	608.4	624.0	563.9

Table **4-2**: Maximum Residual von Mises Stresses

Maximum Residual Von-Mises Stress (MPa)				
	CBS	COS	EDGE	DWL
FUSED	421.5	506.2	504.5	504.0
TAB	444.6	506.0	504.6	502.1
W1S	557.8	593.2	578.1	539.7
SLOT	565.9	594.7	594.4	532.8

Table **4-3**: Maximum Design Load Resultant Shell Displacements

Maximum Resultant Shell Displacement (mm)				
	CBS	COS	EDGE	DWL
FUSED	18.47	13.01	17.86	12.41
TAB	18.88	13.54	18.29	12.74
W1S	21.90	15.97	21.45	14.20
SLOT	23.69	16.93	22.95	14.75

Table **4-4**: Maximum Resultant Displacement Between Stiffeners

Maximum Resultant Displacement Between Stiffeners (mm)				
	CBS	COS	EDGE	DWL
FUSED	4.01	1.04	3.63	2.48
TAB	4.06	1.09	3.60	2.55
W1S	4.78	1.35	4.18	2.59
SLOT	4.77	1.45	4.17	2.45

Table **4-5**: Maximum Design Load Resultant Shell Displacement as Percentage of Stiffener Spacing

Resultant Displacement as % of Stiffener Spacing				
	CBS	COS	EDGE	DWL
FUSED	1.00%	0.26%	0.91%	0.62%
TAB	1.02%	0.27%	0.90%	0.64%
W1S	1.20%	0.34%	1.05%	0.65%
SLOT	1.19%	0.36%	1.04%	0.61%

Table **4-6**: Maximum Residual Resultant Shell Displacements

Maximum Residual Resultant Shell Displacement (mm)				
	CBS	COS	EDGE	DWL
FUSED	1.48	0.11	1.28	0.36
TAB	1.61	0.39	1.37	0.42
W1S	2.58	1.65	2.41	0.95
SLOT	3.08	2.01	3.01	0.99

Table **4-7**: Maximum Residual Resultant Shell Displacements as Percentage of Longitudinal Spacing

Resultant Displacement as % of Longitudinal Spacing				
	CBS	COS	EDGE	DWL
FUSED	0.14%	0.01%	0.12%	0.03%
TAB	0.15%	0.04%	0.13%	0.04%
W1S	0.25%	0.16%	0.23%	0.09%
SLOT	0.29%	0.19%	0.29%	0.06%

Table **4-8**: Maximum Design Load Effective Plastic Strain

Maximum Effective Plastic Strain				
	CBS	COS	EDGE	DWL
FUSED	1.85%	1.09%	1.52%	1.20%
TAB	1.89%	1.84%	1.57%	1.23%
W1S	3.42%	4.23%	4.14%	2.98%
SLOT	3.97%	4.59%	4.78%	2.84%

Table **4-9**: Maximum Residual Effective Plastic Strain

Maximum Residual Effective Plastic Strain				
	CBS	COS	EDGE	DWL
FUSED	1.70%	0.99%	1.20%	0.94%
TAB	1.60%	1.05%	1.22%	0.93%
W1S	2.71%	3.88%	3.31%	2.34%
SLOT	2.94%	3.95%	3.94%	2.07%

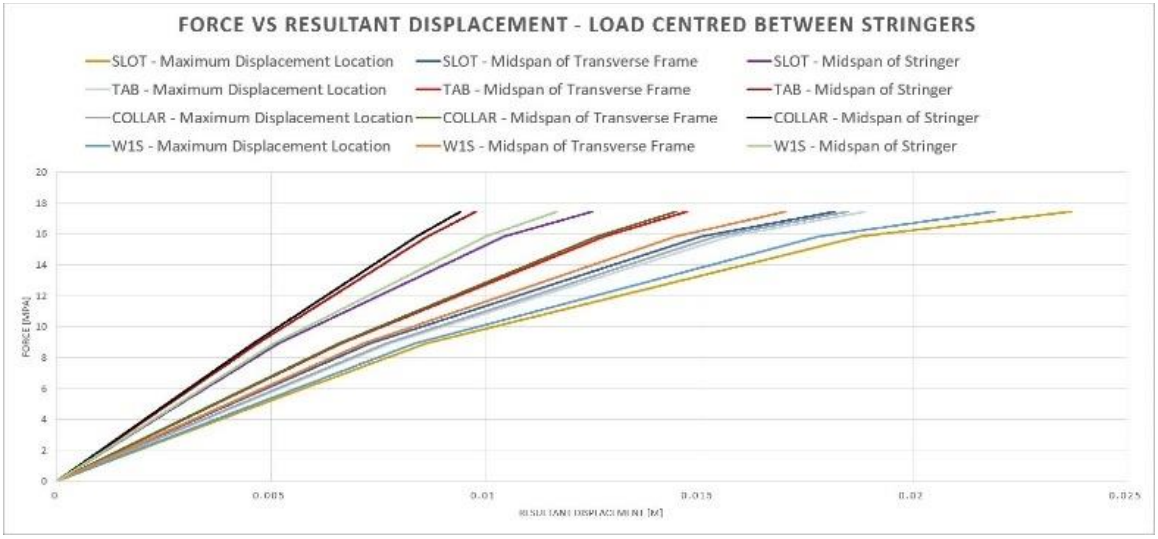

Figure 4-4: Force vs Resultant Displacement - All Penetration Designs - Load Centred Between Stringers

It must be noted that the ABS failure criterion defined as having a permanent deformation of the side shell of greater than 2% of the longitudinal spacing was adhered to by all designs. The residual side shell displacement had a maximum value of 3.08 mm for the slot

connection design for the centred on stringer load location. This represented a 0.29% permanent deformation of the side shell as a percentage of the longitudinal member spacing. The shell displacement between stiffeners also never exceeded the failure criterion of 1.5% of the stiffener spacing. This criterion showed the lowest variability between the penetration designs. The highest percentage value observed was 1.20% for the centred between stringers load location for the welded one side penetration design. The effective plastic strain failure criterion showed a similar pattern to the other criteria. There was a noticeable decrease in structural performance for the welded one side and slot penetrations. These two penetration designs exceeded the failure criterion of 2.5% effective plastic strain for each load location at the design load, and all but the design waterline load location when considering the residual effective plastic strain.

It is also important to consider the stress patterns and general behaviour of primary structural members under the applied load. Polar class rules indicate that plasticity, to a small extent, is acceptable as frames and plates are designed around a plastic collapse mechanism. It was important throughout the analysis of the simulations to check for three-hinge collapse in frames and certain plasticity patterns that indicate undesirable behaviour such as excessive plasticity in main members such as the longitudinal stringers. On that note, stress and out of plane resultant displacement in the longitudinal stringers was checked in both the peak load and residual cases.

Resultant displacement, von Mises stress, and effective plastic strain results for the penetration welded on one side with tab and design waterline load location are shown in Figure 4-5 through Figure 4-7.

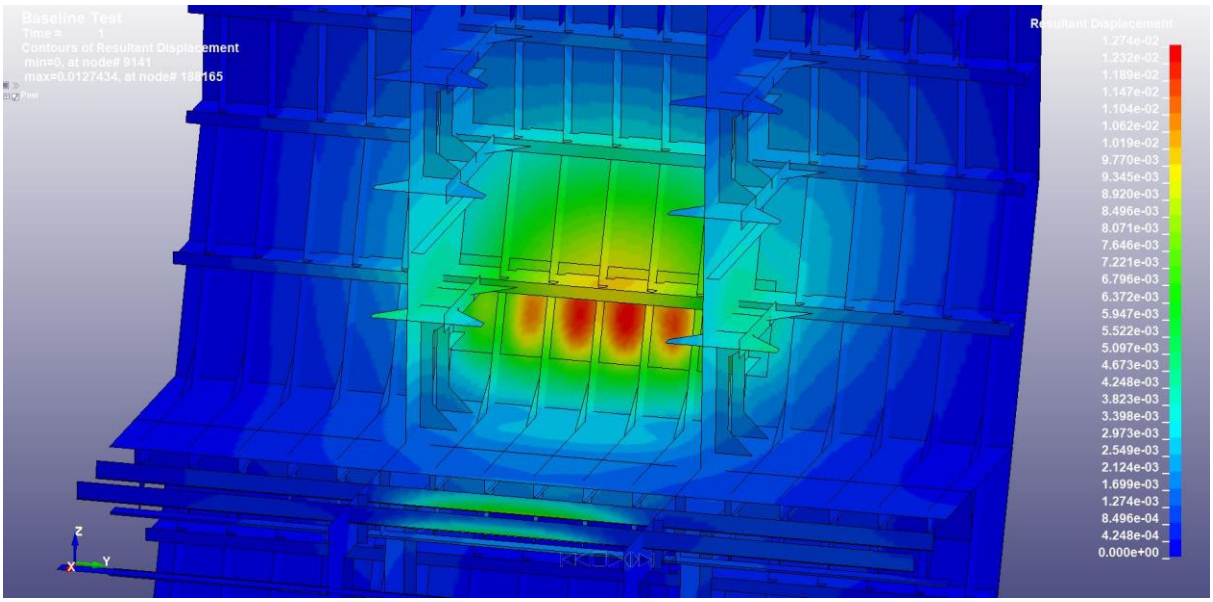

Figure 4-5: Welded One Side With Tab – Design Waterline Load Patch – Resultant Displacement

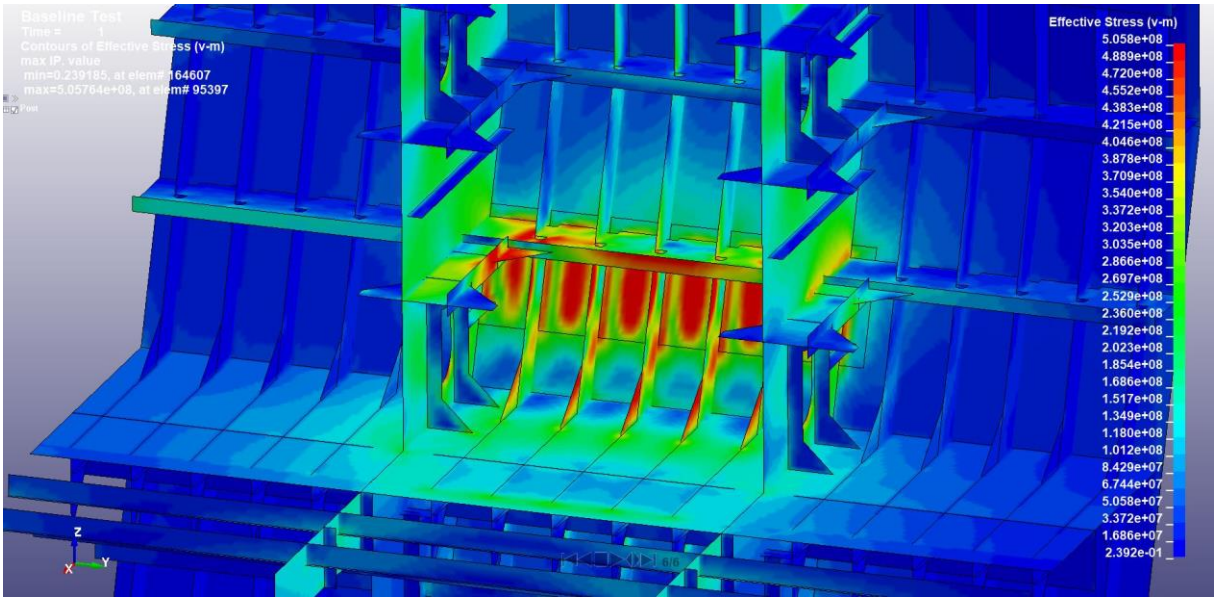

Figure 4-6: Welded One Side With Tab – Design Waterline Load Patch – von Mises Stress

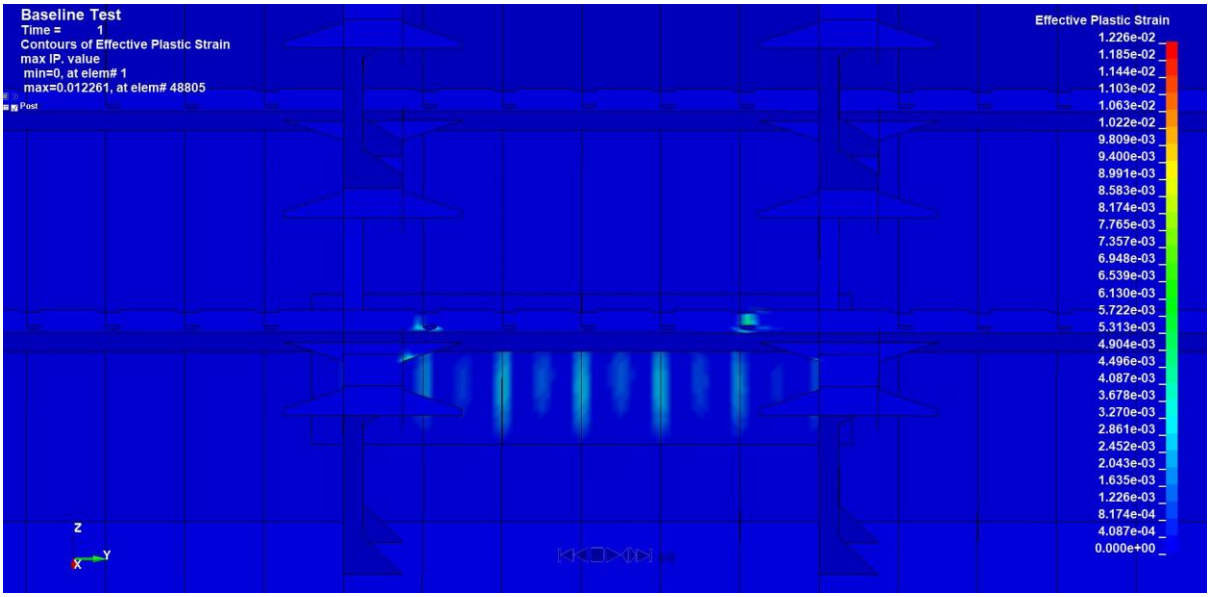

Figure 4-7: Welded One Side With Tab – Design Waterline Load Patch – Effective Plastic Strain

As can be seen from these stress profiles, there is plasticity observed in multiple areas for each run, notably in the web and flange of the longitudinal stringer. However, it should be noted that at the design load, none of the penetration designs at any of the load locations exhibited indication of stiffener/stringer buckling or three-hinge collapse. The maximum out of plane stringer web displacement for the peak load in any run was 5.84 mm. This occurred for the centred between stringers load location with the welded on one side connection design. As for the vertical stiffeners, in none of the runs for any load location or connection design did the out of plane displacement exceed 7 mm.

Considering all failure criteria and the structural performance of each penetration design, it is clear that a penetration welded on one side with a supporting tab is an effective

alternative to a fully welded collar. In none of the simulations did this penetration design exceed any of the three failure criteria presented or show any other undesirable response in the primary structure. This penetration design displayed very similar results to the fully welded collar case across all simulations. The slot and welded one side cases performed similarly to each other, but each showed significantly worse structural responses than the fully welded collar and tab cases. While both the slot and welded one side penetrations passed the shell displacement failure criteria, they each failed the effective plastic strain criterion at the design load for all load locations. As mentioned, this failure criterion has a drawback of depending on element size since smaller elements will resolver higher stresses near stress concentrations. However, specifically for these two penetration designs, the peak plastic strain was always near the curved edge of a penetration and not on an element that would indicate the existence of an abnormally high strain concentration. Because of this, and their noticeably worse performance across the structural responses investigated, these designs were still considered to have failed the outlined criteria.

4.6 Overload

An overload case was also explored in this research however it was not optimized. The load patch was changed, a new model size was not investigated, and an associated mesh convergence analysis wasn't performed. It was a one-time run to explore what an overload case may look like using the same 3-D models, meshes, and LS-PrePost files as the design load cases. It was decided to use a polar class 1 load on the polar class 2 structure. This meant a load patch of slightly larger dimensions and a design pressure of about 1.5 MPa higher than the design load case.

One issue that was made evident right away was that only changing the load patch size and pressure while leaving the remining cards the same was that an implicit solver may not have been ideal for this scenario. As mentioned in the literature review, previous work on overload cases for polar class vessels using LS-Dyna has been done, and in the case of Pearson et al. (2015), an implicit solver was used and there were convergence issues leading to long simulation times. This also proved true for the one case evaluated during this research. The one overload case took over 2 hours and 30 minutes for the slot connection design with the centred between stringers load location while the design load simulation for the same connection design and load location took under 10 minutes. This indicates that an explicit solver may be a better choice if this study was to be repeated.

The results of this simulation showed that this connection design was not suitable for an overload case. Stresses of over 800 MPa were observed while effective plastic strain was observed to reach over 50% on primary stiffening members indicating that fracture was occurring in multiple key locations. Buckling was observed in both the upper and lower stringers while the vertical stiffeners also failed. As this model was not optimized for this exploratory test, there are uncertainties present in the results. Further simulations should be performed on overload cases by adjusting the 3-D models to properly incorporate the larger load patch, perhaps performing another mesh convergence analysis for this new load, and performing simulations with both an implicit and explicit solver. The results presented in this section may be inaccurate due to a variety of reasons. Namely, a new mesh convergence analysis was not performed, and an implicit solver is not likely to be

appropriate. This could cause the resultant displacements, stresses, and strains to not be representative of the true structure.

Chapter 5 Conclusions and Recommendations

5.1 Conclusions

This research focused on using non-linear finite element analysis to analyze various connection designs between vertical stiffeners and longitudinal stringers in the ice-strengthened region of a PC2 vessel with the end goal being to see if designs other than the current industry standard exhibit a level of structural strength that passes the defined failure criteria outlined in this paper. Ultimately it was discovered that there is a connection design that can provide an appropriate level of structural strength that adhere to the failure criteria defined in this thesis and that can be used in place of a fully welded collar. This design would also likely save significant ship construction costs as the shipyard labour would be decreased due to the simpler welding and construction requirements.

Other than the failure criteria outlined previously, stress and strain profiles alongside out of plane displacement of primary members needed to be considered. While these failure criteria involving resultant shell displacement and overall strain values are useful to determine a concise point where a design becomes unacceptable, undesirable trends such as stiffener and stringer buckling and high stress concentrations may not be captured solely by these criteria.

Residual stresses must be taken into account when evaluating the structural integrity of the structure after an ice load. Residual stresses can lead to cracking or warping of the material

over time and are a contributing factor to fatigue over time. It is not desirable to have large areas of residual stress for any of the designs. The largest residual stress values all came with either the welded one side or slot connection design. Residual stresses in these cases exceeded the yield strength of 500 MPa in all but the design waterline load location simulations. For these cases, the peak stress was found to be in the web of the lower stringer near one of the penetrations. This is not a desirable design outcome as tensile residual stresses can contribute to failure over time.

The fully welded collar case is one of the current designs for polar class vessels. This design was expected to exhibit the strongest response of all connection designs. Upon observing the results, it became clear that this was true. If watertight connections are required in the ice belt region of a PC 2 vessel, a fully welded collar is an acceptable design choice as it passes all failure criteria outlined in this thesis. This result served to indicate that the models created were adequate and likely represented the true ship behaviour well. Yield was reached in the stringer web for this case, but stresses, resultant displacements, and effective plastic strains were the lowest for the fully welded collar connection design across all load locations.

The symmetrical slot penetration case showed, overall, the weakest structural response and is not recommended for future shipbuilding strategy in the ice-strengthened region of PC 2 vessels. While it passed the displacement failure criteria, it had high stress concentrations when compared to the fully welded collar and tab simulations. Plus, the stress was much higher and the yield strength was reached in the structure in far more locations.

The same was true for the case with a penetration welded on one side. Again, it passed the displacement criteria, but failed the strain criterion and displayed significant stress concentrations and more yield than the fully welded collar and tab runs.

The penetration welded on one side with a tab was the best performing design outside of the fully welded collar case. It passed all failure criteria outlined in this thesis, exhibited lower von Mises stress values in both the peak load and residual cases, and had a lower peak strain than all runs besides the fully welded collar. This design also saves costs and material over the collared case making the welded on one side with tab case the best option for future ship construction in the ice-strengthened region of a PC2 vessel.

In conclusion, the following recommendations are made for future shipbuilding strategy of polar class vessels: when it comes to the construction of a polar class 2 vessel, specifically the connection region between the main horizontal stringers and vertical stiffeners in the ice belt region of the vessel, it is recommended to consider using a design which includes a typical penetration through the stringer web that is welded to the vertical stiffener on one side with a supporting lug or tab made of steel of the same thickness of the stringer being welded to the vertical stiffener and the stringer web across the penetration. This design proved to provide an acceptable level of structural strength demonstrating that the difference between a fully welded collar and a penetration welded on one side with a tab were comparable as both designs passed all failure criteria presented in this thesis. Based on research regarding polar class vessel cost estimation, this design could also save costs as the total number of weld passes is expected to be lower, though a cost estimation should first be performed. It is not recommended to use either a slot penetration with no supporting

weld at all, nor a penetration welded on one side to the vertical stiffener without a supporting lug or tab. These two designs demonstrated a significantly worse structural performance than the fully welded collar and welded one side with tab case. Both the slot and welded one side case failed the effective plastic strain failure criterion presented in this thesis.

5.2 Recommendations and Future Work

There are multiple aspects of the research done in this thesis that can be expanded upon with future work. One aspect would be to test the connection arrangements on different polar classes. This research focused exclusively on polar class 2, and the results of the research do not necessarily scale proportionally with polar class. This would give the opportunity to look into how steel and cost-saving designs could be applied to lower and potentially non-ice class vessels.

It would also be beneficial to perform more simulations using different connection designs. One suggestion for other designs would be to change the penetration dimensions. The dimensions of the penetrations in this research were chosen largely from industry experience and other designs used on similar ships. There is room to adjust the details. Another idea would be to change the frequency of tab usage on the penetrations. In this research, tabs were added to every single penetration on all stringers in the region of the ship that was modelled. While this arrangement gave the best structural response of all trials other than the current practice of using a fully welded collar around the penetration

region, it is possible that using a different frequency of tabs, such as one every second penetration, could give a similar level of performance while further reducing costs.

Further research could also be done into the effect of including welds within the FEA simulations. This was out of the scope of the work done in this thesis, however responses of the welds themselves could prove to be significant to future design standards. Though including weld models within an FEA analysis can be resource intensive as they would likely need to be modeled as solid elements. Solid elements introduce extra complexities into an FEA model. Solid elements take longer to solve and require extra considerations when modelling as it is a three-dimensional object as opposed to the strictly two-dimensional shell elements used in this research.

The load patch locations could be further adjusted to observe the response of the ice-strengthened regions of the vessel under different scenarios. One such example would be adjusting the model so that the horizontal centre is now on a web frame instead of being between both web frames then applying the load directly to the web frame. This research only focused on changing the vertical position of the load patch, and two of the failure criteria chosen had to do with shell deformation between web frames or longitudinal members. Failure criteria may need to be adjusted if centering the load on a web frame as the side shell deformation would be expected to be less than in this research. Another option would be to apply the load patch along the edge of a web frame. This would be a logical next step to the load locations tested in this research.

A cost analysis of the different connection designs would also be beneficial. While it is known that an increase in welding increases costs significantly, a cost analysis showing the comparison of the strength drawbacks with the lowered construction costs.

Finally, the models used in this thesis should be optimized for testing overload cases. The failure criteria defined in this thesis come from the structural response from the design load, however the structural response of a load of 1.5 times the design load, or a higher polar class load, such as a polar class 1 load, would be interesting to observe. One such run was performed throughout the research phase of this thesis: a load for a PC1 vessel was applied to the slot penetration design with the centred between stringers load location with no other changed made to the model. The run time for this simulation in LS-Dyna took approximately 2 hours and 42 minutes while the design load case took approximately 9 minutes. This is approaching a 20-fold increase in simulation time. This is likely due to using an implicit solver when an explicit solver would have been more appropriate. The simulation time mentioned was heavily influenced by convergence issues that stemmed from the highly nonlinear structural response to the overload. As mentioned earlier in this thesis, explicit solvers are better suited than implicit for simulations involving highly non-linear behaviour, so this simulation should be performed again with an explicit solver. This simulation was done as a test to gauge the time commitment to perform the same simulation for each of the 32 cases outlined in this work. This does not include any 3-D modeling, meshing, or pre-processing in LS-PrePost. These, however, could virtually be eliminated if future work was done with the models already created for this thesis. The task would shift from time consuming modeling to time consuming simulation. Further testing into

the use of an implicit solver vs explicit solver and their simulation times should be done prior to investigating an overload case for this mode

Chapter 6 Bibliography

ABS. (2005). *GUIDANCE NOTES ON ICE CLASS*.

ABS. (2021). *Guidance Notes on Nonlinear Finite Element Analysis of Marine and Offshore Structures 2021*. www.eagle.org

Bobeldijk, M., Dragt, S., Hoogeland, M., & van Bergen, J. (2021). Assessment of the technical safe limit speed of a non-ice-strengthened naval vessel with representative and alternative side shell designs in ice-infested waters. *Ships and Offshore Structures*, *16*(S1), 275–289. https://doi.org/10.1080/17445302.2021.1912475

Bond, J., & Kennedy, S. (1998). Physical Testing and Finite Element Analysis of Icebreaking Ship Structures in the Post Yield Region. *International Offshore and Polar Engineering Conference*, 577–585.

Daley, C. G., Daley, K. H., Dolny, J., & Quinton, B. W. T. (2016). Overload response of flatbar frames to ice loads. *Ships and Offshore Structures*, *12*, S68–S81. https://doi.org/10.1080/17445302.2016.1254520

Daley, C. G., & Hermanski, G. (2005). *Ship Frame/Grillage Research Program Investigation of Finite Element Analysis Boundary Conditions*.

Daley, C. G., & Kendrick, A. (2002). Derivation of plastic framing requirements for polar ships. *Marine Structures*, *15*(6), 543–559. https://doi.org/10.1016/S0951-8339(02)00019-9

Finnish-Swedish Ice Class Rules. (2017). THE STRUCTURAL DESIGN AND ENGINE OUTPUT REQUIRED OF SHIPS FOR NAVIGATION IN ICE.

Hakala, M. K. (1980). A NONLINEAR FINITE ELEMENT ANALYSIS OF AN ICE-STRENGTHENED SHIP SHELL STRUCTURE. In *Computers and Structures* (Vol. 12).

IACS. (2016). *Requirements concerning Polar Class*.

Kõrgesaar, M., Kujala, P., & Romanoff, J. (2018). Load carrying capacity of ice-strengthened frames under idealized ice load and boundary

conditions. *Marine Structures*, *58*, 18–30. https://doi.org/10.1016/j.marstruc.2017.10.011

Leal, M., & Gordo, J. M. (2017). HULL'S MANUFACTURING COST STRUCTURE. *Brodogradnja*, *68*(3), 1–24. https://doi.org/10.21278/brod68301

Lotsberg, I. (2006). Fatigue design of plated structures using finite element analysis. *Ships and Offshore Structures*, *1*(1), 45–54. https://doi.org/10.1533/saos.2005.0006

LSTC. (2011). *LS-DYNA Database Binary Output Files*.

LSTC. (2022). *LS-DYNA Keyword User's Manual*. *1*.

Miroyannis, A. (2005). *Estimation of Ship Construction Costs.* http://Iibraries.mit.edu/docs

Moakler, E. (2018). *DEVELOPMENT OF GUIDELINES FOR TRANSVERSE WEB FRAME DESIGN IN POLAR CLASS SHIPS USING NON LINEAR FINITE ELEMENT ANALYSIS*.

Normore, S. S. (2007). *Cost Reduction of Polar Class Vessels: Structural Optimization that Includes Production Factors.*

Okada, T., & Kawamura, Y. (2018). *Strength evaluation of intersection between stiffeners and primary supporting members considering the effect of shear force on the primary member web*.

Pearson, D., Hindley, R., & Crocker, J. (2015). *Icebreaker Grillage Structural Interaction and the Characteristic Stiffness Curve*. http://onepetro.org/snamewmtc/proceedings-pdf/WMTC15/1-WMTC15/D011S003R002/2509950/sname-wmtc-2015-159.pdf/1

Quinton, B. W. T., Daley, C. G., Gagnon, R. E., & Colbourne, D. B. (2016). Guidelines for the nonlinear finite element analysis of hull response to moving loads on ships and offshore structures. *Ships and Offshore Structures*, *12*, S109–S114. https://doi.org/10.1080/17445302.2016.1261391

Ross, J. M. (2004). A Practical Approach for Ship Construction Cost Estimating. *International Conference on Computer and IT Applications in the Maritime Industries (COMPIT'04)*, 98–110.

Valtonen, V., Bond, J., & Hindley, R. (2020). Improved method for non-linear FE analysis of polar class ship primary structures. *Marine Structures*, *74*. https://doi.org/10.1016/j.marstruc.2020.102825

Wang, B., Yu, H.-C., & Basu, R. (2008). *Ship and Ice Collision Modeling and Strength Evaluation of LNG Ship Structure.* https://doi.org/10.1115/OMAE2008-57134

Appendix A Flow Curve Data for HS36 and HS51 Steels

HS36		
True Strain ε *[%]*	*True Plastic Strain* $\varepsilon_p=\varepsilon-\sigma/E$ *[%]*	*True Stress* σ *[N/mm²]*
0.000	0.000	0.000
0.169	0.000	355.600
0.499	0.329	356.775
0.829	0.659	357.955
1.159	0.988	359.138
1.489	1.318	360.325
1.861	1.685	369.970
2.233	2.053	379.713
2.606	2.420	389.551
2.978	2.788	399.473
3.878	3.677	423.558
4.779	4.567	446.402
5.680	5.459	465.522
6.581	6.353	480.019
7.481	7.248	491.330
8.382	8.144	501.090
9.283	9.041	510.216
10.184	9.937	519.131
11.084	10.834	528.024
11.985	11.730	536.980

HS36		
True Strain ε ***[%]***	***True Plastic Strain*** $\varepsilon_p=\varepsilon-\sigma/E$ ***[%]***	***True Stress*** σ ***[N/mm²]***
12.886	12.627	546.044
13.787	13.523	555.239
14.687	14.419	564.578
15.588	15.316	572.641
16.489	16.215	577.584
17.390	17.113	582.303
18.290	18.012	586.819
19.191	18.910	591.150
20.092	19.809	595.313
20.993	20.708	599.321
21.893	21.607	603.185
22.794	22.506	606.917
23.695	23.405	610.526
24.596	24.304	614.021
25.496	25.203	617.409
26.397	26.102	620.697
27.298	27.001	623.891
28.199	27.901	626.997
29.099	28.800	630.021
30.000	29.699	632.966

HS51		
True Strain ε ***[%]***	***True Plastic Strain*** $\varepsilon_p=\varepsilon-\sigma/E$ ***[%]***	***True Stress*** σ ***[N/mm²]***
0.000	0.000	0.000
0.238	0.000	501.190
0.551	0.312	502.760
0.863	0.624	504.335
1.176	0.936	505.915
1.489	1.248	507.500
1.861	1.614	520.302
2.233	1.980	533.227
2.606	2.346	546.234
2.978	2.712	559.151
3.878	3.600	587.219
4.779	4.491	606.351
5.680	5.386	619.522
6.581	6.281	630.847
7.481	7.177	641.762
8.382	8.072	652.669
9.283	8.968	663.692
10.184	9.863	674.876
11.084	10.761	681.297
11.985	11.659	686.788
12.886	12.558	691.920
13.787	13.456	696.739

HS51		
True Strain ε ***[%]***	***True Plastic Strain*** $\varepsilon_p=\varepsilon-\sigma/E$ ***[%]***	***True Stress*** σ ***[N/mm²]***
14.687	14.355	701.284
15.588	15.253	705.586
16.489	16.152	709.669
17.390	17.051	713.558
18.290	17.950	717.269
19.191	18.849	720.821
20.092	19.748	724.225
20.993	20.647	727.496
21.893	21.547	730.642
22.794	22.446	733.675
23.695	23.345	736.602
24.596	24.245	739.431
25.496	25.144	742.168
26.397	26.044	744.820
27.298	26.943	747.392
28.199	27.843	749.889
29.099	28.742	752.315
30.000	29.642	754.675